Mechanism of the Efficient Tryptophan Fluorescence Quenching in Human γD-Crystallin Studied by Time-Resolved Fluorescence[†]

Jiejin Chen,[‡] Dmitri Toptygin,[§] Ludwig Brand,*[,§] and Jonathan King*[,‡]

Department of Biology, Massachusetts Institute of Technology, Cambridge, Massachusetts 02139, and Department of Biology, Johns Hopkins University, Baltimore, Maryland 21218

Received March 23, 2008; Revised Manuscript Received June 19, 2008

ABSTRACT: Human γD-crystallin (HγD-Crys) is a two-domain, β-sheet eye lens protein found in the lens nucleus. Its long-term solubility and stability are important to maintain lens transparency throughout life. HγD-Crys has four highly conserved buried tryptophans (Trps), with two in each of the homologous β-sheet domains. In situ, these Trps will be absorbing ambient UV radiation that reaches the lens. The dispersal of the excited-state energy to avoid covalent damage is likely to be physiologically relevant for the lens crystallins. Trp fluorescence is efficiently quenched in native HγD-Crys. Previous steady-state fluorescence measurements provide strong evidence for energy transfer from Trp42 to Trp68 in the N-terminal domain and from Trp130 to Trp156 in the C-terminal domain [Chen, J., et al. (2006) *Biochemistry 45*, 11552−11563]. Hybrid quantum mechanical−molecular mechanical (QM-MM) simulations indicated that the fluorescence of Trp68 and Trp156 is quenched by fast electron transfer to the amide backbone. Here we report additional information obtained using time-resolved fluorescence spectroscopy. In the single-Trp-containing proteins (Trp42-only, Trp68-only, Trp130-only, and Trp156-only), the highly quenched Trp68 and Trp156 have very short lifetimes, $\tau \sim 0.1$ ns, whereas the moderately fluorescent Trp42 and Trp130 have longer lifetimes, $\tau \sim 3$ ns. In the presence of the energy acceptor (Trp68 or Trp156), the lifetime of the energy donor (Trp42 or Trp130) decreased from ∼3 to ∼1 ns. The intradomain energy transfer efficiency is 56% in the N-terminal domain and is 71% in the C-terminal domain. The experimental values of energy transfer efficiency are in good agreement with those calculated theoretically. The absence of a time-dependent red shift in the time-resolved emission spectra of Trp130 proves that its local environment is very rigid. Time-resolved fluorescence anisotropy measurements with the single-Trp-containing proteins, Trp42-only and Trp130-only, indicate that the protein rotates as a rigid body and no segmental motion is detected. A combination of energy transfer with electron transfer results in short excited-state lifetimes of all Trps, which, together with the high rigidity of the protein matrix around Trps, could protect HγD-Crys from excited-state reactions causing permanent covalent damage.

Crystallins are the predominant structural proteins found in the vertebrate eye lens. The α-, β-, and γ-crystallins have a critical role in maintaining human eye lens transparency. α-Crystallins are major structural proteins but also function as molecular chaperones forming large polydisperse multimers and interacting with non-native proteins to prevent them from aggregation (*1, 2*). The oligomeric β- and the monomeric γ-crystallins function solely as structural proteins. The β- and γ-crystallins both contain four homologous Greek key motifs organized into two domains. Most crystallin proteins are synthesized during embryonic development, with little protein turnover in adulthood (*3*), and therefore crystallins have to remain stable and soluble throughout life. Cataract, the most common cause of blindness worldwide, represents the aggregation of oxidatively damaged partially unfolded proteins. Covalently damaged crystallins, including HγD-Crys,[1] accumulate in the insoluble fraction separated from cataractous lenses (*4*−*6*). Oxidized tryptophan residues in HγD-Crys have been identified in aged cataractous human lens by mass spectrometry (*7*).

HγD-Crys is the second most abundant γ-crystallin of the lens nucleus, the region formed earliest in eye development (*3, 8*). HγD-Crys is a monomeric, 173 amino acid protein. The crystal structure of HγD-Crys has been solved to 1.25 Å resolution (*9*). It is composed of β-sheets arranged in four Greek key motifs separated into two highly homologous domains (Figure 1). Each domain has two buried intrinsic

[†] Supported by National Institutes of Health Grant GM 17980 and NEI Grant EY 015834 to J.K. and NSF Grant MCB-0416965 to L.B.

* Authors to whom correspondence should be addressed. Phone: (410) 516-7298 (L.B.); (617) 253-4700 (J.K.). Fax: (410) 516-5213 (L.B.); (617)-252-1843 (J.K.). E-mail: ludwig.brand@jhu.edu; jaking@mit.edu.

[‡] Massachusetts Institute of Technology.

[§] Johns Hopkins University.

[1] Abbreviations: HγD-Crys, human γD-crystallin; Trps, tryptophans; QM-MM, hybrid quantum mechanics−molecular mechanics; UV, ultraviolet; ET, electron transfer; FRET, Förster resonance energy transfer; TCSPC, time-correlated single-photon counting; IRF, impulse response function; DAC, decay-associated spectra; TAC, time-to-amplitude converter; MCA, multichannel analyzer; N-td, N-terminal domain; C-td, C-terminal domain; TRES, time-resolved emission spectrum; TRA, time-resolved fluorescence anisotropy; CT, charge transfer; MD, molecular dynamics.

10.1021/bi800499k CCC: $40.75
Published on Web 09/17/2008

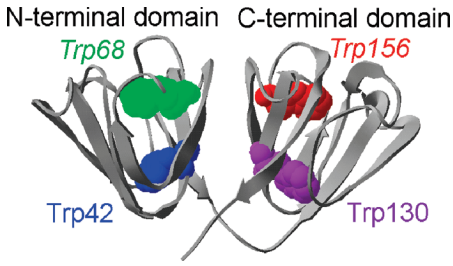

FIGURE 1: The crystal structure of wild-type HγD-Crys depicted in ribbon representation showing the four intrinsic tryptophans in spacefill, Trp42 and *Trp68* in the N-terminal domain, and Trp130 and *Trp156* in the C-terminal domain (Protein Data Bank code: 1HK0).

Trps, Trp42 and Trp68 in the N-terminal domain and Trp130 and Trp156 in the C-terminal domain. These four Trps are conserved through all the vertebrate β- and γ-crystallins. To help the reader keep track of the special relationships among these four tryptophans, we will write the two efficiently quenched *Trp68* and *Trp156* in italics. The other two moderately fluorescent Trp42 and Trp130 will be in regular style.

Ultraviolet (UV) radiation is one of the risk factors for the age-related cataracts (*10*). Although only a small percent of the solar UV light can reach the eye, ocular lenses are continuously exposed to ambient UV radiation with wavelengths from 295 to 400 nm, which could cause cumulative photochemical damage (*11*). UV radiation with the wavelength of 300 nm is most detrimental to the eye lens in animal models (*12, 13*). Within proteins, only aromatic residues, primarily Trp and Tyr, absorb at 300 nm, and the Trp residue contributes the most to the absorbance at this wavelength (*14*). The photochemical reactions of Trps in crystallin proteins may play a key role in cataractogenesis (*11, 15*). The absorption of a photon by a Trp residue promotes the Trp side chain to an electronically excited state. At ambient temperature, the excited Trp side chain can take part in a photodamage reaction (*16*), or it can emit a fluorescence photon, or it can transfer its excitation to another Trp, or it can lose its excitation due to a nonradiative quenching mechanism. There is a competition among these pathways of an excited-state Trp residue. Both steady-state and time-resolved fluorescence measurements provide valuable information about fluorescence lifetimes, energy transfer, and quenching processes (*14, 17*).

Steady-state fluorescence from the four Trps in HγD-Crys has been studied in considerable detail (*18*). In its native state HγD-Crys is less fluorescent than in its denatured state. In other words, the fluorescence of the native state HγD-Crys is quenched. Fluorescence quenching in the native state was also found in other β- and γ-crystallins (*19*−*23*). The quantum yields of the individual Trps in HγD-Crys have been measured using single-Trp-containing proteins with the other three Trp residues replaced by Phe (*18*). The triple mutants, each containing three Trp to Phe substitutions and one native Trp, will be here referred to as Trp42-only, *Trp68-only*, Trp130-only, and *Trp156-only*, respectively. Trp42-only and Trp130-only are moderately fluorescent, with quantum yields of 0.13 and 0.17, respectively. In contrast, *Trp68*-only and *Trp156-only* are extremely quenched, with the quantum yields of only about 0.01.

Hybrid quantum mechanical−molecular mechanics (QM-MM) simulations strongly indicate that the highly efficient quenching of *Trp68* and *Trp156* is due to fast electron transfer from the indole ring to the amide backbone (*18*). Nearby water molecules and surrounding polar residues stabilize the charge transfer state. The QM-MM method used to compute the electron transfer process was developed recently by Callis et al. (*24*−*29*). The differences in the quantum yields between Trp42 and *Trp68* in the N-terminal domain, and between Trp130 and *Trp156* in the C-terminal domain, can be explained by the different rates of electron transfer from the indole ring to a local amide. A negative (positive) charge will decrease (increase) the quantum yield if it is closer to the indole ring than to the electron acceptor because these arrangements stabilize (destabilize) the charge transfer state (*24*−*29*). In the case of HγD-Crys, the electrostatic stabilization is much greater for *Trp68* (or *Trp156*) than for Trp42 (or Trp130). The theoretical predictions based on this effect are consistent with the quantum yields measured experimentally.

Steady-state fluorescence experiments provided evidence that Förster resonance energy transfer (FRET) also contributes to the quenching of Trp fluorescence in HγD-Crys (*18*). There is energy transfer from Trp42 to *Trp68* in the N-terminal domain and from Trp130 to *Trp156* in the C-terminal domain. If the energy acceptor (*Trp68* or *Trp156*) is substituted by Phe, the fluorescence intensity of the single Trp to Phe mutant (W68F or W156F) exceeds that of the wild-type HγD-Crys. In contrast, the substitution of the energy donor (Trp42 or Trp130) results in a decreased intensity of the single mutant (W42F or W130F) compared to wild type. The comparison of steady-state fluorescence intensities of the triple Trp to Phe mutants (Trp42-only, *Trp68-only*, Trp130-only, and *Trp156-only*) and the double Trp to Phe mutants (Trp42/*Trp68* and Trp130/*Trp156*) further confirmed the presence of intradomain energy transfer (*18*).

Absorption of a UV photon by a Trp residue in crystallin promotes the side chain of that Trp to an electronically excited state, in which it can remain for several nanoseconds. While the Trp side chain is in the excited state, it can undergo an irreversible chemical reaction, resulting in covalent damage to the protein. It is thus important to be able to measure for how long each Trp residue remains in the excited state. Time-resolved fluorescence measurements give a precise answer to this question. A few time-resolved fluorescence studies have been reported for bovine crystallins. Borkman described time-resolved studies of bovine α-crystallins and γB-crystallin (*30, 31*), which contain two and four Trp residues, respectively. However, the authors did not address the question of the lifetimes of the individual Trp residues and whether they change in the presence of the other Trp residues or not. In the case of resonance energy transfer the lifetime of the donor is different in the absence and in the presence of the acceptor. In this paper we describe a time-resolved fluorescence study of all triple and double Trp to Phe substitutions of HγD-Crys, which was designed to measure the donor lifetimes in the absence and in the presence of the acceptors.

Nanosecond and picosecond time-resolved fluorescence measurements have considerable advantages over the steady-state measurements. The rates of resonance energy transfer and other excited-state reactions can be measured directly

in a time-resolved study. If the time resolution is combined with spectral resolution, then it becomes possible to tell the difference between a homogeneous ensemble of excited-state fluorophores in relaxing environments and a heterogeneous ensemble of excited-state fluorophores in static environments (*32*). This capability is very important in application to Trp fluorescence in proteins, because some proteins relax on the nanosecond time scales. For a protein with a single Trp and a single conformation it is possible to measure picosecond and nanosecond relaxation dynamics of the protein matrix (*33*). For a protein containing multiple Trps in different environments it is possible to separate the spectra corresponding to different lifetimes (*34*), which may provide a significant help in assigning multiple lifetimes to multiple chromophores. In the present study we explore all of the capabilities of time-resolved fluorescence mentioned above.

A different kind of dynamic information can be obtained when the time resolution is combined with polarized fluorescence measurements (*17*). Time-resolved anisotropy measurements make it possible to tell the difference between the Brownian rotation of a globular protein as a whole and the segmental motion within the protein (*17*). This provides a method of studying protein integrity, and this method has been applied in this paper.

MATERIALS AND METHODS

Mutagenesis, Expression, and Purification of Proteins. Double and triple tryptophan to phenylalanine substitutions were constructed by site-directed mutagenesis (*35*). Primers (IDT-DNA) encoding the substitutions were used to amplify the gene for HγD-Crys with an N-terminal His_6 tag in a pQE.1 plasmid (*35*). The double mutation W68F/W130F, which was named as Trp42/*Trp156* in the text, was constructed by using the primer encoding the W130F substitution to amplify the W68F mutant plasmid. Other double mutants W68F/W156F, W42F/W130F, and W42F/W156F were created by an analogous procedure. All of the mutations were confirmed by DNA sequencing (Massachusetts General Hospital). The double mutants were named according to the remaining tryptophans present (Trp42/*Trp68*, Trp130/*Trp156*, Trp42/*Trp156*, *Trp68*/Trp130, Trp42/Trp130, and *Trp68*/*Trp156*). The triple tryptophan to phenylalanine substitutions were also named for the remaining native tryptophan (Trp42-only, *Trp68-only*, Trp130-only, and *Trp156-only*).

Wild-type and mutant HγD-Crys proteins were expressed and purified as described by Kosinski-Collins et al. (*35*). The proteins were expressed by *Escherichia coli* M15 [pREP4] cells. All of the mutant proteins expressed at levels similar to wild type and accumulated as native and soluble proteins. The proteins were purified by affinity chromatography using a Ni-NTA resin (Qiagen) as previously described (*35*). The purities of the proteins were confirmed by SDS−PAGE. Concentrations of purified proteins were calculated from absorbance data at 280 nm using extinction coefficients computed by ProtParam tool (ExPASy) based on the amino acid composition (*36*). The extinction coefficient was 23970 cm^{-1} M^{-1} for triple tryptophan mutants, 29660 cm^{-1} M^{-1} for double tryptophan mutants, and 41040 cm^{-1} M^{-1} for wild-type HγD-Crys.

Time-Resolved Fluorescence Intensity and Anisotropy Measurements. All fluorescence measurements were carried out in S buffer (10 mM sodium phosphate buffer, 5 mM DTT, and 1 mM EDTA at pH7.0) at the temperature of 20 °C. Different protein concentrations were used for HγD-Crys mutants with different numbers of Trp residues, so that the concentration of Trp residues was about 80 μM in each protein sample. Time-correlated single-photon counting (TCSPC) data were obtained using a home-built instrument described previously (*33*). To minimize the excitation of tyrosine residues, we tuned the exciting wavelength to 300 nm. To minimize Trp photobleaching and subsequent contamination of the fluorescence signal by the emission from the photoproducts, the exciting power was attenuated to 50 μW or less, and the exciting beam was defocused so that the power density did not exceed 25 $\mu W/mm^2$. Photons were registered by two identical wings in T format. In each wing fluorescence emission passed through a polarizer and a monochromator and was detected by a microchannel plate photomultiplier. In time-resolved anisotropy measurements the polarizers in two wings were set at 0° and 90° from the vertical. The monochromators were tuned to 345 nm, which excluded the highly polarized Raman scatter (peak near 333 nm) from the 8 nm bandwidth. In time-resolved intensity measurements both polarizers were set at 55° from the vertical. The monochromators were scanned from 310 to 440 nm with 5 nm steps. At each of the 27 emission wavelengths, fluorescence photons were counted for 300 s by both wings simultaneously. Impulse response function (IRF) was recorded quasi-simultaneously (15 s IRF recording after each 75 s of fluorescence recording) using a Ludox scatterer cell and had a full width of 65 ps at half-maximum. This represents the time resolution of the entire system.

Steady-State Fluorescence and Absorption Measurements. After each time-resolved intensity measurement, a steady-state fluorescence emission spectrum was taken with the same protein sample, using the same exciting wavelength and temperature, on an SLM-48000 fluorometer (SLM Instruments, Urbana, IL). The monochromator bandwidths were 2 nm for the excitation and 4 nm for the emission. The steady-state spectra were corrected for both the spectral variation of the emission channel sensitivity and the inner filter effect as described earlier (*32*). The corrected spectra were then used in renormalizing the preexponential amplitudes resulting from the global analysis of the time-resolved data (vide infra). An UV absorption spectrum of each protein sample was taken both before the beginning of the time-resolved and after the end of the steady-state fluorescence measurements. The two spectra were then compared, since a difference could indicate Trp photobleaching or protein aggregation. No significant changes in the absorption spectrum during the course of fluorescence measurements were found with any of the proteins studied in this work.

Analysis of Time-Resolved Intensity Data. Each time-resolved fluorescence intensity curve was fitted by a numerical convolution of the quasi-simultaneously acquired IRF with the following model function:

$$F_m(t) = b_m + s_m\delta(t) + \theta(t)\sum_{n=1}^{N_{exp}} \alpha_{mn} \exp(-t/\tau_n) \qquad (1)$$

The index m is relevant to the global analysis only, representing the serial number of the wavelength stop at which the emission was collected. $\delta(t)$ and $\theta(t)$ are Dirac delta and Heaviside step functions, respectively. N_{exp} denotes

the total number of exponentials. b_m, s_m, α_{mn}, and τ_n are free fitting parameters. b_m is the photomultiplier background (dark counts). s_m is the intensity of scattered exciting radiation (including Raman). α_{mn} is a preexponential amplitude, and it is allowed to be positive or negative. τ_n represents a time constant. A nonlinear weighted least-squares algorithm was used to minimize χ^2. The weights were calculated based on the Poissonian photon statistics. The quality of the fits was judged by the reduced χ^2 values, by plots of weighted residuals, and by the autocorrelation plots. The confidence intervals for the values of the fitting parameters were calculated using the diagonal elements of the inverted Hessian matrix, as described by Hamilton (*37*).

Single-Curve Analysis. For the single-curve analysis we added up the time-resolved intensity data obtained at several emission wavelengths. This significantly improved the signal-to-noise ratio and made it possible to resolve more exponential terms. The data were fitted by a numerical convolution of the IRF with the model function similar to that in eq 1, but without the index *m*. The best values of the fitting parameters *b*, *s*, α_n, and τ_n were determined by the program TCPHOTON (*33*).

Global Analysis. Trp fluorescence usually cannot be adequately fit by the monoexponential function, even in proteins containing a single Trp residue (*17*). Complex time-resolved Trp fluorescence in proteins has its origin either in heterogeneity or in an excited-state interaction, such as protein relaxation on the nanosecond time scale (*32*). In either case, it is expected that the preexponential amplitudes (α_i) are emission wavelength dependent, but the time constants (τ_i) are wavelength independent (*33*). It is thus appropriate to use global analysis (*38*) to analyze the data obtained at all wavelengths simultaneously, with the values of τ_i constrained to be the same at all wavelengths while the values of α_i allowed to be positive or negative and different at different wavelengths. In the experiments described here, data were obtained at 27 emission wavelengths with a total of about 80 million photons being counted. In the global analysis we used all of these photon counts. In addition, global analysis by its very nature has a higher resolving power than single curve analysis (*38*). It is thus not surprising that up to six exponentials could be resolved in the global analysis of some single- and double-Trp-containing proteins, which would not be possible if we used single-curve analysis to fit the data obtained at just one emission wavelength.

In the case of the global analysis the lifetimes τ_n played the role of the global fitting parameters, with same values for all 27 emission wavelengths, whereas the amplitudes α_{mn} and other parameters (b_m, s_m) played the role of the local fitting parameters, with different values for every emission wavelength. The best values of all fitting parameters were found by the program L_GLOBAL (*33*). After the global fitting, the values of the amplitudes corresponding to every emission wavelength were renormalized so that the sum of the products $\alpha_{mn}\tau_n$ would be equal to the steady-state fluorescence emission intensity measured at the emission wavelength number *m*. Technical details of this renormalization, polynomial interpolation of the discrete preexponential amplitude spectra, conversion of the spectra between wavelength and wavenumber scales, and conversion from the preexponential amplitude spectra to time-resolved emission spectra were described previously (*32*).

Analysis of Time-Resolved Anisotropy Data. Vertical and horizontal polarization components of the time-resolved emission intensity were fitted by the model described elsewhere (*32*). In this model the time-resolved anisotropy was represented by the following function:

$$r(t) = \sum_{m=1}^{N_{ani}} \beta_m \exp(-t/\varphi_m) \quad (2)$$

The fitting parameters β_m and ϕ_m are the amplitudes and correlation times for the exponential terms involved in the deconvoluted time-resolved anisotropy function. Only the values of these parameters were of interest to us. The description of other fitting parameters, which represented total fluorescence emission intensity and experimental artifacts, can be found elsewhere (*32*).

Reversible Förster Resonance Energy Transfer Rates. If a protein contains two Trp residues, then the emission spectrum of each Trp residue will have at least some overlap with the absorption spectrum of the other Trp residue; therefore, reversible energy transfer is possible. The rates of the forward (k_{12}) and reverse (k_{21}) energy transfer can be determined using the following equations (*39*):

$$k_{12} = \frac{(\lambda_1 - k_1)(\lambda_2 - k_1)}{k_2 - k_1} \quad (3)$$

$$k_{21} = \frac{(\lambda_1 - k_2)(\lambda_2 - k_2)}{k_1 - k_2} \quad (4)$$

In these equations k_1 represents the decay rate of Trp1 in the absence of Trp2, $k_1 = 1/\tau_1$, where τ_1 is the lifetime of Trp1 in the absence of Trp2. Likewise, k_2 and τ_2 ($k_2 = 1/\tau_2$) are the decay rate and the lifetime of Trp2 in the absence of Trp1, respectively. In the case where both Trps are present, two exponentials with the new time constants (τ_1' and τ_2') should be observed. The time constants τ_1' and τ_2' may not be attributable to individual Trp residues, since the decay of each Trp residue is described by the biexponential law. Parameters λ_1 and λ_2 in eqs 3 and 4 are defined as the inverses of the time constants τ_1' and τ_2'; i.e., $\lambda_1 = 1/\tau_1'$ and $\lambda_2 = 1/\tau_2'$.

If the time-resolved fluorescence emission of Trp1 alone and/or Trp2 alone is not monoexponential, then the approach of Potter (*39*) described above is not applicable. The equations to be used in this case of multiexponential fluorescence depend on the specific mechanism.

The approach we used in this work is based on the assumption that each Trp residue has only one conformation, consistent with the crystal structure of HγD-Crys. This means that, for each Trp pair, there is a definite value for donor−acceptor distance, κ^2, forward energy transfer rate k_{12}, and reverse rate k_{21}. Multiexponential fluorescence may have its origin in the time-variant rate of a nonradiative decay process, such as electron transfer from the excited-state Trp to the protein backbone (*18*). We also assumed that the amplitude-weighted mean lifetime of each Trp is wavelength invariant. This assumption was verified experimentally, and only insignificant spectral variation of the mean lifetime was found. Under these assumptions the amplitude-weighted mean lifetimes of Trp1 and Trp2 can be substituted for τ_1 and τ_2, which can be then used to calculate the values of k_1 and k_2 in eqs 3 and 4. Definition of τ_1 and τ_2 may still be

ambiguous since it requires assignment of all the time constants to either Trp1 or Trp2. This assignment becomes possible in the case where one of the decay rates, for instance, k_2, is much greater than the other decay rate, k_1, and also much greater than both energy transfer rates, k_{12} and k_{21}. It is not difficult to show that in this case all of the time constants resolved in the fluorescence of the double-Trp-containing protein (Trp1/Trp2) will be either of the order of $1/k_2$ (attributable to Trp2) or much longer than $1/k_2$ (attributable to Trp1). We have to emphasize that this approach is applicable only in the cases where the mean lifetime of one Trp residue is at least an order of magnitude longer than the mean lifetime of the other Trp residue.

Calculation of the Förster Resonance Energy Transfer Efficiencies. The efficiency of Förster resonance energy transfer (FRET) was originally defined for the irreversible transfer. For the reversible energy transfer we use the following definitions of the energy transfer efficiency (*40*):

$$E_{12} = \frac{k_{12}}{k_1 + k_{12}} \tag{5}$$

$$E_{21} = \frac{k_{21}}{k_2 + k_{21}} \tag{6}$$

In this work the efficiency of energy transfer was measured experimentally and also calculated theoretically based on the Förster equation (*41*). The experimental values of the FRET efficiency were calculated from the experimental values of k_1, k_2, k_{12}, and k_{21} using eqs 5 and 6. The decay rate constant k_1 or k_2 was calculated as the inverse amplitude-weighted mean lifetime of Trp1 or Trp2 in the absence of the other Trp residue. The experimental energy transfer rates k_{12} and k_{21} were obtained using eqs 3 and 4.

The theoretical values of energy transfer efficiency were calculated from the Förster radii R_0 and the distances R between the centers of the donor and the acceptor (*41*):

$$E_{\text{theor}} = \frac{{R_0}^6}{{R_0}^6 + R^6} \tag{7}$$

The values of R were determined from the crystal structure of HγD-Crys as described in the following section. The values of R_0 were determined using the Förster equation (*41*):

$${R_0}^6 = \frac{9\ln(10)}{128\pi^5 n^4 N_A}\kappa^2 Q_D J \tag{8}$$

N_A is Avogadro number. κ^2 is the orientation factor determined from the crystal structure of HγD-Crys. Q_D is the quantum yield of the donor in the absence of the acceptor. J is the overlap integral. n is the refractive index of the medium. For n we used the value of 1.3567, which represents the refractive index of water at $\lambda = 308.2$ nm and $T = 20$ °C (*42*). Q_D values have been reported previously (*18*). The values of the overlap integral were determined using the following equation:

$$J = \frac{\int c_1 \varepsilon_A(\lambda) {c_2}^4 \lambda^4 F_D(\lambda)\, d\lambda}{\int F_D(\lambda)\, d\lambda} \tag{9}$$

Here $c_1 = 1000$ cm^3/L and $c_2 = 10^{-7}$ cm/nm are unit conversion factors. $\epsilon_A(\lambda)$ is the decadic molar extinction coefficient of the energy acceptor. $F_D(\lambda)$ is the corrected emission spectrum of the donor. The integration was carried out over the spectral range from 286 to 456 nm, which completely included the emission spectrum of the donor.

The absorption spectra of the acceptors were measured using *Trp68-only* and *Trp156-only* for the energy transfer in the forward direction and using Trp42-only and Trp130-only for the energy transfer in the reverse direction. The absorption values were converted to extinction coefficient values using the molar extinction coefficients of these mutants at 280 nm, which were calculated as described in Mutagenesis, Expression, and Purification of Proteins. The extinction coefficient of 14 tyrosine residues was subtracted from the extinction coefficient of each single-Trp HγD-Crys variant prior to the calculation of the overlap integral. The shape of the tyrosine absorption spectrum in a protein was modeled using the absorption spectrum of *N*-acetyltyrosineamide in ethanol (the polarity of protein interior is closer to that of ethanol than to that of water). To make sure that the correct amount of tyrosine absorption is subtracted, we renormalized the experimental tyrosine extinction coefficient spectrum to the value of 1280 M^{-1} cm^{-1} at $\lambda = 280$ nm that was also used in calculating the extinction coefficient of the protein (the extinction coefficient of Trp was assumed to be 5690 M^{-1} cm^{-1} at this wavelength) (*36*). The contribution of cystines and phenylalanines was not subtracted from the protein absorption spectrum because all measurements were carried out at reducing conditions, while cysteines and phenylalanines do not absorb appreciably at $\lambda > 280$ nm.

The emission spectra of the donors were measured using Trp42-only and Trp130-only for the energy transfer in the forward direction and using *Trp68-only* and *Trp156-only* for the energy transfer in the reverse direction. The conditions are described in the section Steady-State Fluorescence and Absorption Measurements. The use of the 300 nm exciting wavelength prevented us from measuring the emission intensity at $\lambda < 306$ nm. The Trp emission spectra were extended to $\lambda < 306$ nm using the emission spectrum of 3-methylindole in cyclohexane−dioxane solvent mixture (83:17) (*18*). At $\lambda > 306$ nm the emission spectrum of 3-methylindole matched the emission spectra of single-Trp-containing proteins very well. The spectra were corrected for the spectral sensitivity variation of the instrument as described earlier (*32*) and used to calculate the overlap integral.

Determination of R and κ^2 from the Protein Crystal Structure. The values of R and κ^2 were calculated from the crystal structure of HγD-Crys (PDB code: 1HK0) in two steps. First, the radius vectors $\vec{r}$ describing the coordinates of all fluorophore centers and the unit vectors $\vec{u}$ describing the directions of all electronic transition were calculated by a computer program. The output of the program is included in the Table 1S in Supporting Information. The program determines the directions of the transition moments ^1L_a and ^1L_b for Trp relative to the indole nuclear frame using the information from Callis (*43*). For the center of a Trp fluorophore the program takes the point at the middle of the bond connecting atoms CD2 and CE2.

Second, for selected Trp pairs and only for the electronic transitions involving the excited state ^1L_a, we calculated the following vectors and scalars:

$$\vec{R} = \vec{r}_D - \vec{r}_A \quad (10)$$

$$R = \sqrt{(\vec{R}\cdot\vec{R})} \quad (11)$$

$$\kappa^2 = [(\vec{u}_D\cdot\vec{u}_A) - 3R^{-2}(\vec{R}\cdot\vec{u}_D)(\vec{R}\cdot\vec{u}_A)]^2 \quad (12)$$

Here $\vec{r}_D$ and $\vec{r}_A$ are the radius vectors describing the absolute coordinates of the centers of the donor and the acceptor. $\vec{R}$ is a vector connecting the center of the donor with the center of the acceptor. $(\vec{a}\cdot\vec{b})$ denotes the scalar product of the vectors $\vec{a}$ and $\vec{b}$. R is the distance between the centers of the donor and the acceptor. $\vec{u}_D$ and $\vec{u}_A$ are the unit vectors parallel to the directions of the $^1L_a \leftrightarrow {}^1A$ transition dipole moments for the donor and the acceptor. κ^2 is the orientation factor, which enters in the Förster equation. The values of R and κ^2 are shown in the Table 2S in Supporting Information. The choice of exclusively $^1L_a \leftrightarrow {}^1A$ transitions for Trp−Trp energy transfer calculations is dictated by the following two considerations. First, it is known that fluorescence emission from Trp residues in all proteins is entirely due to the $^1L_a \rightarrow {}^1A$ transition (*44*). Second, it is also known that the red tail ($\lambda > 295$ nm) in the absorption spectrum of Trp, which is responsible for the overlap between the absorption and emission spectra of Trp, is mainly due to the $^1A \rightarrow {}^1L_a$ transition (*45*).

RESULTS

Global Analysis of Time-Resolved Intensity Data. Time-resolved fluorescence intensity data were collected from a set of purified wild-type and mutant HγD-Crys proteins. The data obtained at all wavelengths were analyzed by global analysis simultaneously. The results of the global analysis include the reduced χ^2, a set of time constants τ_i, and a set of preexponential amplitude spectra $\alpha_i(\lambda)$ or $\alpha_i(\nu)$, where λ and ν represent the emission wavelength and wavenumber, respectively. Figure 2 shows the preexponential amplitude spectra of Trp130-only HγD-Crys on a linear wavelength scale. Four exponential terms were required to obtain an adequate fit for this protein (reduced $\chi^2 = 1.01$). Between four and six exponential terms were required for adequate global fits to the data obtained with the other three single-Trp-containing proteins, six double-Trp-containing proteins, and wild-type HγD-Crys. Corresponding preexponential amplitude spectra are shown in Figures 1S−10S in Supporting Information. 95% confidence intervals for the values of the preexponential factors α_{mn} are depicted as error bars in these figures. For all but the fastest exponentials with $\tau <$ 0.2 ns, the 95% confidence intervals are so narrow that the gap between the upper and the lower error bar can be either barely visible or invisible.

The origin of the multiple exponential terms can be in heterogeneity or relaxation or in a combination of the two. To distinguish between heterogeneity and relaxation, we relied on the shape conservation criterion introduced and tested elsewhere (*32, 33*). Figure 3 demonstrates the application of this heterogeneity criterion to the case of Trp130-only HγD-Crys. For homogeneous solutions of fluorophores in viscous solvents (*46*) and for single-Trp-containing proteins undergoing nanosecond scale relaxation in the excited state (*32, 33*), the shape of the instantaneous emission spectrum should be time-invariant except for a parallel shift along the wavenumber axis. A variation in the shape of the instantaneous emission spectrum indicates the presence of heterogeneity, which is a result of emission from different fluorophores (e.g., Tyr and Trp) or from the same fluorophore in different environments (e.g., buried and solvent-exposed Trp residues). Although the instantaneous emission spectra in Figure 3 differ from one another very little, their shape is not conserved, which indicates the presence of heterogeneity.

As an example of shape variation consider the instantaneous spectra at 0 and 0.40 ns after excitation. The 0.40 ns

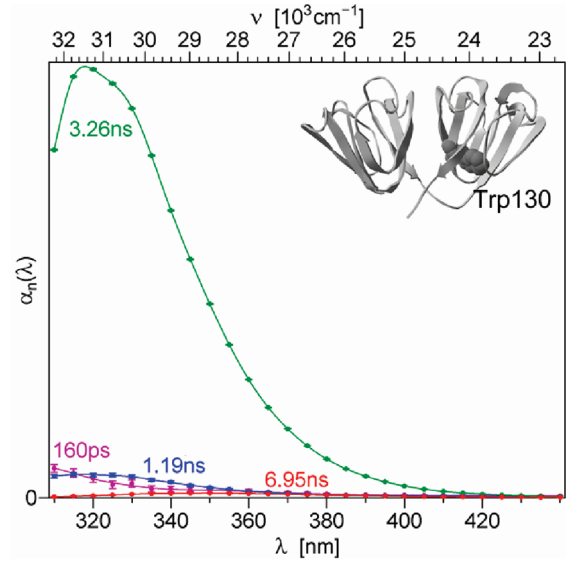

FIGURE 2: Preexponential amplitude spectra $\alpha_i(\lambda)$ obtained by the global analysis of the fluorescence emission from Trp130-only HγD-Crys. The ribbon structure of wild-type HγD-Crys with Trp130 in spacefill is shown at the upper right corner. The values of the corresponding time constants τ_i are shown near each spectrum using a matching color. The spectra have been renormalized using a corrected steady-state emission spectrum as described in Materials and Methods.

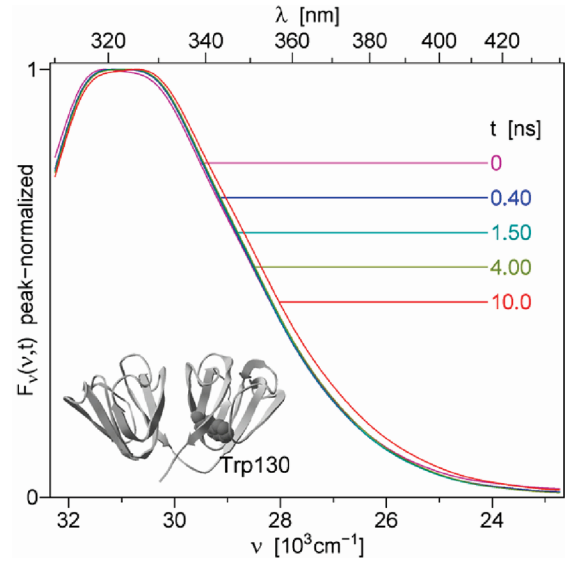

FIGURE 3: Instantaneous fluorescence emission spectra of Trp130-only at different times after excitation. These spectra were reconstructed from the preexponential amplitude spectra shown in Figure 2 and peak-normalized to facilitate shape comparison. The ribbon structure of wild-type HγD-Crys with Trp130 in spacefill is shown at the bottom. The spectra shown in the figure correspond to the following times after excitation: 0 ns (purple), 0.40 ns (blue), 1.50 ns (dark cyan), 4.00 ns (yellow-green), and 10.0 ns (red). The spectra are plotted on a linear wavenumber scale. A wavelength scale is shown at the top of the figure.

Table 1: Lifetimes (τ_i), Fractional Amplitudes (α_i %), and Fractional Intensity Contributions (f_i %) for the Single- and Double-Trp-Containing Proteins with Both Trp Residues in the Same Domain and the Wild-Type HγD-Crys[a]

	protein	τ_1, ns (α_1 %, f_1 %)	τ_2, ns (α_2 %, f_2 %)	τ_3, ns (α_3 %, f_3 %)	τ_4, ns (α_4 %, f_4 %)	χ^2
Trps in N-terminal domain	Trp42-only	−[b]	−	1.72 (25, 18)	**2.85**[c] (68, 80)	1.00
	Trp68-only	**0.061** (68, 31)	**0.14** (30, 33)	−	−	1.02
	Trp42/*Trp68*	**0.084** (51, 7)	−	0.48 (10, 7)	**1.31** (37, 75)	1.06
Trps in C-terminal domain	Trp130-only	−	−	−	**3.26** (91, 96)	1.01
	Trp156-only	**0.050** (36, 13)	**0.12** (54, 46)	0.27 (9, 17)	−	1.01
	Trp130/*Trp156*	**0.080** (58, 14)	0.23 (17, 11)	−	**0.94** (24, 66)	1.03
	wild type	**0.065** (44, 6)	0.16 (23, 8)	0.82 (17, 32)	1.41 (15, 47)	1.01

[a] The lifetimes were obtained by the global analysis of the time-resolved fluorescence data from all 27 emission wavelengths. The amplitudes $\alpha_i(\lambda)$ and intensity contributions $f_i(\lambda) = \alpha_i(\lambda)\tau_i$ were integrated over the emission wavelength range from 320 to 340 nm and then renormalized to a unit sum. The fractional amplitudes (α_i %) and fractional intensity contributions (f_i %) were shown in parentheses following the corresponding lifetime. [b] Some minor components with $\alpha\% < 3\%$ or $f\% < 2\%$ were not listed above in order to simplify the table. [c] The dominant lifetimes with $\alpha\% > 30\%$ and/or $f\% > 60\%$ were shown in boldface.

spectrum (blue line) has a flat top, which is probably a result of a superposition of two unresolved peaks (unresolved vibrational structure). In the case of the 0 ns spectrum (purple line) the peak on the left is slightly taller than the peak on the right. The purple curve and the blue curve cannot be superimposed by means of a parallel shift along the wavenumber axis, which reveals the contribution of heterogeneity (emission from multiple fluorophores). Since the instantaneous spectra at 0.40 ns (blue line), 1.50 ns (cyan line), and 4.00 ns (green-yellow line) are practically identical, the contribution from the fluorophore that is responsible for the difference between the 0 and 0.40 ns spectra decays completely by $t = 0.40$ ns. In Figure 2 we see only one exponential component with τ shorter than 0.40 ns; its spectrum is shown by the purple line. On the basis of the heterogeneity test we know that the fluorophore responsible for the 160 ps component is not the same fluorophore that is dominant at 0.40, 1.50, and 4.00 ns. Trp130 is most likely the dominant fluorophore in Trp130-only HγD-Crys; therefore, the 160 ps component is associated with a fluorophore other than Trp130. The peak of the spectrum associated with the 160 ps exponential lies at the emission wavelength less than 310 nm. Since the tyrosine emission peak is near 300 nm and HγD-Crys contains 14 tyrosine residues, it is likely that tyrosine emission is the source of the 160 ps component. The small amplitude of the 160 ps component is a result of 300 nm excitation, which is not optimum for exciting tyrosine residues. When we excited Trp130-only HγD-Crys at 296 nm, the relative contributions of the 160 ps and 1.19 ns components were found to be significantly greater, consistent with more efficient excitation of tyrosine at 296 nm as compared to 300 nm (results not shown). This points to the fact that the 1.19 ns component may also be due to tyrosine emission (at least in part).

A difference in shape is also observed between the instantaneous spectra at 4.00 and 10.0 ns. Neither the spectral variation between 0 and 0.40 ns nor that between 4.00 and 10.0 ns can be attributed to protein and/or solvent relaxation around Trp130, since this mechanism cannot explain the variation in the spectral shape. The 10.0 ns spectrum is wider than the 4.00 ns spectrum; therefore, the two spectra cannot be superimposed by means of a parallel shift along the wavenumber axis. Since the wide spectrum is always more heterogeneous than the narrow one, this reveals the presence of heterogeneity in the 10 ns spectrum. This heterogeneity can only be explained in terms of a long-lifetime fluorophore that outlives the main fluorophore in Trp130-only HγD-Crys and becomes a significant contributor at $t = 10$ ns. Among the exponential components shown in Figure 2 there is only one component with a τ longer than that of the dominant component. The spectrum associated with the τ of 6.95 ns has its maximum at 350 nm, and its shape closely resembles the spectra of solvent-exposed Trp residues in proteins. It is possible that the 6.95 ns component results from a small fraction of HγD-Crys in the unfolded state or from another trace contaminant protein.

The dominant component with $\tau = 3.26$ ns clearly represents the emission of the main fluorophore in Trp130-only HγD-Crys, which is Trp130. The fractional mean amplitude $\alpha\%$ of the 3.26 ns component in the spectral range from 320 to 340 nm equals 91% (see Table 1).

Lifetimes of Trp Residues in Single-Trp-Containing Proteins and Double-Trp-Containing Proteins with Both Trp Residues in the Same Domain. The amplitude spectra shown in Figure 2 and in Supporting Information (Figures 1S−10S) contain no negative amplitudes, and therefore there is no direct evidence of an excited-state reaction or dielectric relaxation (*32*). In the absence of dielectric relaxation and excited-state reactions the time constants τ_i represent the lifetimes of excited-state fluorophores. Using the information contained in the shapes of the preexponential amplitude spectra and time-resolved emission spectra, we were able to assign each lifetime to a Trp residue in the native state HγD-Crys (peak near 320 nm), to tyrosine residues (peak <310 nm), or to a trace contaminant (peak near 350 nm). The lifetimes attributable to Trp residues in HγD-Crys are shown in Table 1. The table also gives the values of fractional mean amplitudes (α_i) averaged over the spectral range from 320 to 340 nm and the values of fractional mean steady-state intensity contributions ($f_i = \alpha_i\tau_i$) averaged over the same spectral range. The spectral range from 320 to 340 nm was chosen to minimize the contributions from tyrosine residues ($\lambda < 320$ nm) and solvent-exposed Trp residues in trace contaminant proteins ($\lambda > 340$ nm). To emphasize the dominant components, in Tables 1 and 2 we highlighted the lifetimes with the fractional amplitudes greater than 30% and/or with the fractional intensity contributions greater than 60%.

In single-Trp-containing proteins the highly quenched *Trp68* and *Trp156* (*18*) showed two or three short lifetimes between 0.05 and 0.27 ns. In contrast, the moderately fluorescent Trp42 and Trp130 had much longer lifetimes. A

Table 2: Decay Constants of the Double-Trp-Containing Proteins with Two Trps in the Different Domains[a]

protein	τ_1, ns (α_1 %, f_1 %)	τ_2, ns (α_2 %, f_2 %)	τ_3, ns (α_3 %, f_3 %)	χ^2
Trp42/*Trp156*	**0.085**[b] (57, 6)	1.75 (9, 20)	**2.83** (19, 67)	1.03
Trp68/Trp130	**0.065** (52, 3)	–[c]	**3.15** (29, 89)	1.04
Trp42/Trp130	–	1.77 (22, 14)	**3.12** (73, 84)	1.03
Trp68/*Trp156*	**0.058** (52, 24)	**0.13** (43, 46)	0.32 (4, 11)	1.03

[a] The lifetimes were obtained by the global analysis of the time-resolved fluorescence data from all 27 emission wavelengths. The amplitudes $\alpha_i(\lambda)$ and intensity contributions $f_i(\lambda) = \alpha_i(\lambda)\tau_i$ were integrated over the emission wavelength range from 320 to 340 nm and then renormalized to a unit sum. The fractional amplitudes (α_i %) and fractional intensity contributions (f_i %) were shown in parentheses following the corresponding lifetime. [b] The dominant lifetimes with $\alpha\% > 30\%$ or $f\% < 60\%$ were shown in boldface. [c] Some minor components with $\alpha\% < 3\%$ or $f\% < 5\%$ were not listed above in order to simplify the table.

single lifetime of 3.26 ns can be attributed to Trp130, while two lifetimes of 1.72 and 2.85 ns can be attributed to Trp42, with the 2.85 ns lifetime being dominant.

In the double-Trp-containing proteins, with both Trp residues either in the N-terminal domain (Trp42/*Trp68*) or in the C-terminal domain (Trp130/*Trp156*), we observed one or two short lifetimes ($\tau < 0.3$ ns) attributable to the highly quenched *Trp68* or *Trp156* and one or two longer lifetimes ($\tau > 0.3$ ns) attributable to the moderately fluorescent Trp42 or Trp130. The lifetimes attributable to Trp42 and Trp130 became significantly shorter in the presence of *Trp68* and *Trp156*, respectively. The shortening of the Trp42 and Trp130 lifetimes can be either due to the intradomain Förster resonance energy transfer from Trp42 to *Trp68* and from Trp130 to *Trp156* or due to some other mechanism, such as a change in the Trp environment resulting from a different structure of the mutated protein; however, in a previous study the structure of HγD-Crys was found to be unaffected by the Trp to Phe mutations (*35*).

The rationale of attributing all the lifetimes shorter than 0.3 ns to *Trp68* or *Trp156* and all the lifetimes longer than 0.3 ns to Trp42 or Trp130 was based not only on the values of the corresponding lifetimes in the single-Trp-containing proteins but also on the shapes of the corresponding preexponential amplitude spectra (Figures 1S−10S in Supporting Information). For example, the shape of the spectrum corresponding to the $\tau = 1.31$ ns component in the double-Trp-containing protein, Trp42/*Trp68* (Figure 3S in Supporting Information), closely resembles the shape of the spectrum corresponding to the $\tau = 2.85$ ns component in Trp42-only protein (Figure 1S in Supporting Information), while the shape of the spectrum corresponding to the $\tau = 0.48$ ns component in the Trp42/*Trp68* protein (Figure 3S) closely resembles the shape of the spectrum corresponding to the $\tau = 1.72$ ns component in Trp42-only protein (Figure 1S). The peaks of all the spectra corresponding to $\tau < 0.3$ ns (*Trp68* and *Trp156*) were shifted slightly to the red relative to those corresponding to $\tau > 0.3$ ns (Trp42 and Trp 130). The red shift probably has its origin in the environment of *Trp68* and *Trp156* being more polar than that of Trp42 and Trp130, which is consistent with crystal structure of HγD-Crys and the results of QM-MM calculations (*18*).

Due to the fundamental limit on the number of exponential terms that can be resolved from experimental data, the total number of the resolved lifetimes in the double-Trp-containing protein (e.g., Trp42/Trp130) may differ from the sum of the numbers of lifetimes in the corresponding two single-Trp-containing proteins (e.g., Trp42-only and Trp130-only). Thus, it is not feasible to trace how much each of the individual lifetimes is changed by the presence of the second Trp residue in the same domain. The values of the amplitude-weighted mean lifetimes should be compared in the case where the number of lifetimes attributed to the same Trp is different between the single-Trp- and double-Trp-containing protein. The mean lifetime of Trp42 alone equaled 2.55 ns. In the presence of *Trp68* (the acceptor) the mean lifetime of Trp42 (the donor) decreased to 1.13 ns, which was a 56% decrease. The mean lifetime of *Trp68* alone equaled 0.086 ns, and it became 0.084 ns in the presence of Trp42. Since the difference between 0.086 and 0.084 ns was less than their estimated standard deviation (±0.01 ns), we cannot accurately quantify the effect of Trp42 on the lifetime of *Trp68*.

A similar pattern was observed in the C-terminal domain. Here the lifetime of Trp130 alone (energy donor) was 3.26 ns, and it decreased to 0.94 ns in the presence of *Trp156* (energy acceptor), which was a 71% decrease. The mean lifetime of Trp156 alone equaled 0.106 ns, and it became 0.113 ns in the presence of Trp130. Because the difference was less than the estimated standard deviation (±0.01 ns), it was not a significant change.

Since the single-Trp-containing proteins have a total of eight lifetimes attributable to Trp residues (Table 1), one would expect to see eight lifetimes in the wild-type HγD-Crys, which has all four Trp residues. However, due to the limited number of exponential terms that can be resolved from experimental data, we see only four lifetimes attributable to Trp residues in the wild-type protein (Table 1). The dominant lifetime equaled 0.065 ns, which was associated with the fractional amplitude of 44%. The 0.065 and 0.16 ns lifetimes represent unresolved fluorescence signals from both *Trp68* and *Trp156*. The 0.82 and 1.41 ns lifetimes represent unresolved fluorescence signals from both Trp42 and Trp130.

Figures 4 and 5 show deconvoluted fluorescence intensity on a logarithmic scale, as a function of time. These semilog plots are for illustrative purposes only and were not used to judge the quality of fits to experimental data by model functions, since it is virtually impossible to see minute systematic deviations on a semilog plot (*47*). In Figure 4 the time-resolved emission from Trp42-only protein is almost a straight line except at $t < 0.5$ ns, suggesting that between 0.5 and 8 ns the time-resolved fluorescence appears to be monoexponential. The steep slope and significant curvature of the line of *Trp68-only* protein (green solid line) reveal exceptionally fast and nonmonoexponential decay of *Trp68*. The time-resolved intensity of the double-Trp-containing protein, Trp42/*Trp68*, exhibits two main phases. The steep slope at $t < 0.2$ ns can be attributed to the fast decay of *Trp68*. At $t > 0.2$ ns we observed a decrease in the slope; however, at $t > 0.5$ ns the slope of the broken line (Trp42/

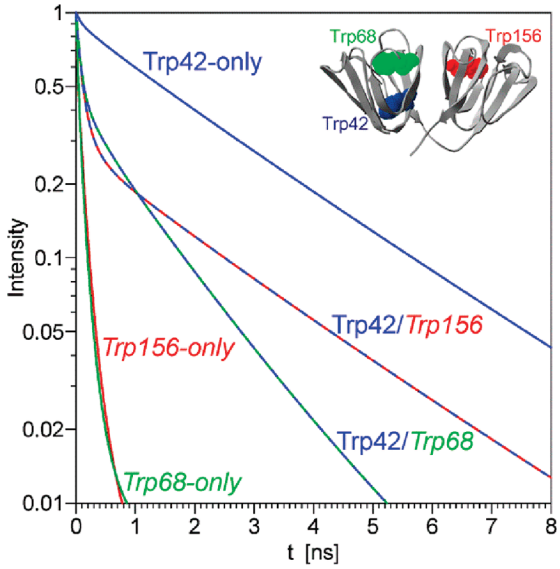

FIGURE 4: Deconvoluted fluorescence intensity in the emission wavelength range from 320 to 340 nm as a function of time after δ excitation for Trp42-only (blue solid line), *Trp68-only* (green solid line), Trp42/*Trp68* (blue-green broken line), *Trp156-only* (red solid line), and Trp42/*Trp156* (blue-red broken line) of HγD-Crys. The ribbon structure of wild-type HγD-Crys with Trp42 (blue), *Trp68* (green), and *Trp156* (red) in spacefill is shown at the upper right corner.

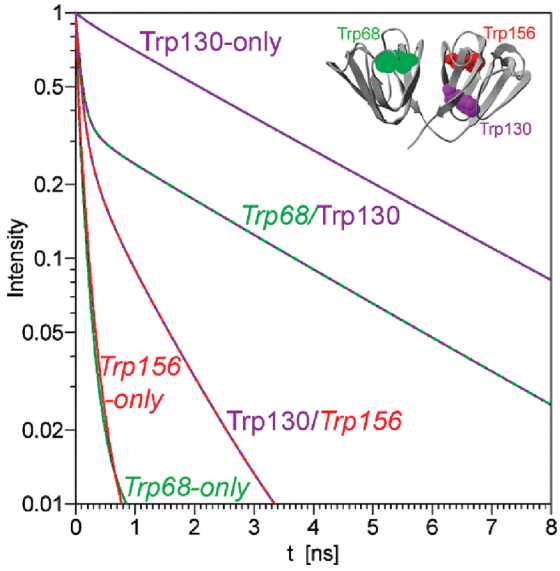

FIGURE 5: Deconvoluted fluorescence intensity in the emission wavelength range from 320 to 340 nm as a function of time after δ excitation for Trp130-only (violet solid line), *Trp156-only* (red solid line), Trp130/*Trp156* (violet-red broken line), *Trp68-only* (green solid line), and *Trp68*/Trp130 (green-violet broken line) of HγD-Crys. The ribbon structure of wild-type HγD-Crys with *Trp68* (green), Trp130 (violet), and *Trp156* (red) in spacefill is shown at the upper right corner.

Trp68) is still considerably steeper than that of the solid line (Trp42-only). This indicates that the decay rate of Trp42 is increased by the energy transfer from Trp42 to *Trp68* or by some other quenching mechanism that is active only in the presence of *Trp68*. If there were no interaction between these two Trps, one would expect the solid line (Trp42-only) and the broken line (Trp42/*Trp68*) to be parallel at $t > 0.5$ ns. This was indeed found in the cases where little or no energy transfer was expected (Trp42-only and Trp42/*Trp156* in Figures 4 and Trp130-only and *Trp68*/Trp130 in Figure 5 described in the next section.)

The time-resolved emission from the Trps in the C-terminal domain (Figure 5) shows very similar trends as those of the Trps in the N-terminal domain. The difference between the slopes of the violet-red broken line (Trp130/*Trp156*) and violet solid line (Trp130-only) in Figure 5 is greater than the difference between the slopes of the blue-green broken line (Trp42/*Trp68*) and blue solid line (Trp42-only) in Figure 4. The slope of a decay curve on a semilog plot represents the decay rate, which equals $k_r + k_{nr}$ in the absence of the acceptor and $k_r + k_{nr} + k_{ET}$ in the presence of the acceptor. Here k_r is the radiative decay rate, k_{nr} is the nonradiative decay rate, and k_{ET} is the energy transfer rate. Thus, if we assume that the Trp to Phe substitutions did not change the values of k_r and k_{nr}, then the difference between the slope of the broken line (Trp42/*Trp68* or Trp130/*Trp156*) and the slope of the solid line (Trp42-only or Trp130-only) equals the energy transfer rate (k_{ET}). This suggests that the rate of energy transfer between Trp130 and *Trp156* in the C-terminal domain is greater than the rate of energy transfer between Trp42 and *Trp68* in the N-terminal domain. The donor−acceptor pair with the greater energy transfer rate also has greater energy transfer efficiency.

Lifetimes for Double-Trp-Containing Proteins with the Two Trps in the Different Domains. Time-resolved and spectrally resolved fluorescence data were also obtained for four double-Trp-containing proteins with the two Trps in the different domains. These mutants can be used as controls to further confirm the energy transfer observed in the mutants with both Trps in the same domain. Since for any combination of one Trp in the N- and one in the C-terminal domain the distance between the centers of the two Trps is greater than 18 Å, little or no energy transfer is expected. The mutants Trp42/*Trp156* and *Trp68*/Trp130 contain one moderately fluorescent Trp (Trp42 or Trp130) and one highly quenched Trp (*Trp68* or *Trp156*). The Trp42/Trp130 mutant contains two moderately fluorescent Trps, whereas the *Trp68*/*Trp156* mutant contains two highly quenched Trps. The lifetimes, fractional amplitudes, and fractional intensity contributions for the four mutants with the Trps in the different domains are shown in Table 2. The lifetimes of the Trp42/*Trp156* protein can be simply assigned to Trp42 and *Trp156* based on the lifetimes of Trp42 alone and *Trp156* alone. The 2.83 ns lifetime can be attributed to Trp42, since it is very close to the dominant lifetime of Trp42 alone (2.85 ns; see Table 1). The 0.085 ns lifetime has very high amplitude ($\alpha\% = 85\%$) and can be attributed to *Trp156*. Similarly, the 3.15 ns lifetime of the *Trp68*/Trp130 protein can be attributed to Trp130 that has a 3.26 ns lifetime in the absence of *Trp68*, and the 0.065 ns component can be attributed to *Trp68*.

Trp42/Trp130 contains two moderately fluorescent Trp residues. The 3.12 ns lifetime represents the unresolved mixture of the 2.85 ns lifetime from Trp42 alone and the 3.26 ns lifetime from Trp130 alone. The 1.77 ns lifetime can be assigned to Trp42 that exhibits a 1.72 ns lifetime when it is alone (see Trp42-only in Table 1), while the Trp130-only protein does not contain a close lifetime. *Trp68*/*Trp156* contains two highly quenched Trp residues. It exhibits two lifetimes (0.058 and 0.13 ns) that represent an

Scheme 1: Reversible Förster Resonance Energy Transfer between Trps in HγD-Crys

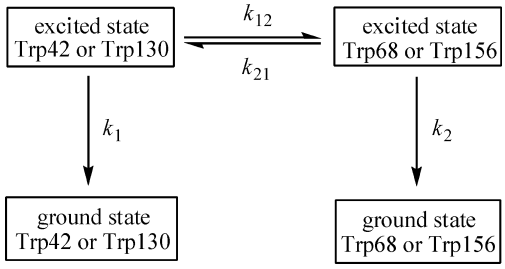

unresolved mixture of two lifetimes from *Trp68-only* (0.061 and 0.14 ns) and two lifetimes from *Trp156-only* (0.050 and 0.12 ns).

Figures 4 and 5 show the time-resolved fluorescence intensity for some double-Trp-containing proteins with the Trp residues in the different domains. The time-resolved emission from the Trp42/*Trp156* protein (the blue-red broken line) consists of a fast phase ($t < 0.5$ ns) and a slow phase ($t > 0.5$ ns) (Figure 4). The slope of the slow phase of Trp42/*Trp156* is nearly identical to that of the Trp42-only protein (the blue solid line). Two straight lines with identical slopes on the semilog scale correspond to two exponentials with equal lifetimes. This suggests that the lifetime of Trp42 is the same in the presence and in the absence of *Trp156*; therefore, there is little or no energy transfer between Trp42 and *Trp156*. Similarly, from the data shown in Figure 5 it follows that there is little or no energy transfer between *Trp68* and Trp130 in the double-Trp-containing protein, *Trp68*/Trp130.

Reversible Förster Resonance Energy Transfer Rates. The shortening of the lifetimes of Trp42 and Trp130 in the presence of *Trp68* and *Trp156* can be explained either in terms of Förster resonance energy transfer or in terms a change in the Trp environment resulting from a different structure of the mutated protein. In a previous study the structure of HγD-Crys was found to be unaffected by the Trp to Phe mutations (*35*). In this work we examine the role of Förster resonance energy transfer in the reduction of Trp42 and Trp130 lifetimes by calculating the rates and efficiencies of the energy transfer rates from the lifetime data and comparing these experimental values with those calculated theoretically using Förster theory. If Förster resonance energy transfer is responsible for the reduction of Trp42 and Trp130 lifetimes, then the experimental and theoretical rates/efficiencies should be in good agreement.

Reversible Förster resonance energy transfer between two Trps is illustrated in Scheme 1. The rates of the forward (k_{12}) and reverse (k_{21}) energy transfer have been calculated for two pairs of Trps, for Trp42 and *Trp68* in the N-terminal domain as well as for Trp130 and *Trp156* in the C-terminal domain. We use index 1 for the moderately fluorescent Trps (Trp42 and Trp130) and 2 for the highly quenched Trps (*Trp68* and *Trp156*), and therefore k_{12} always describes energy transfer from a moderately fluorescent Trp to a highly quenched Trp, while k_{21} always describes energy transfer from a highly quenched Trp to a moderately fluorescent Trp. From eq 4 it follows that k_{21} is directly proportional to ($\lambda_2 - k_2$), where k_2 is the inverse mean lifetime of the highly quenched Trp in the absence of the moderately fluorescent Trp and λ_2 is the inverse mean lifetime of the highly quenched Trp in the presence of the moderately fluorescent Trp. The technical details of calculating the mean lifetime for each Trp are described in Supporting Information. From experimental data we obtained the following values and standard deviations: for Trp42/*Trp68* $k_2 = 11.6 \pm 1.3$ ns^{-1} and $\lambda_2 = 12.0 \pm 1.4$ ns^{-1}; for Trp130/*Trp156* $k_2 = 9.4 \pm 0.9$ ns^{-1} and $\lambda_2 = 8.9 \pm 0.8$ ns^{-1}. Within experimental errors the values of λ_2 and k_2 are equal; therefore, the differences ($\lambda_2 - k_2$) do not significantly differ from zero and so do the rates k_{21}. The k_{21} values calculated using eq 4 are 0.4 ± 1.9 ns^{-1} for Trp42/*Trp68* and -0.5 ± 1.1 ns^{-1} for Trp130/*Trp156*. The negative k_{21} value makes no physical sense; however, since the absolute values of k_{21} are less than the standard deviations in both cases, we conclude that the reverse energy transfer rate is small and cannot be accurately calculated from our experimental data.

If $k_{21} = 0$ and $\lambda_2 = k_2$ within experimental errors, then the term ($\lambda_2 - k_1$) in the numerator of the fraction on the right-hand side of eq 3 cancels out with the term ($k_2 - k_1$) in the denominator and the equation can be reduced to the following:

$$k_{12} = \lambda_1 - k_1 \tag{13}$$

Using the reduced equation we obtained the following forward transfer rates: 0.51 ± 0.09 ns^{-1} for Trp42/*Trp68* and 0.70 ± 0.09 ns^{-1} for Trp130/*Trp156*.

Förster Resonance Energy Transfer Efficiencies. The theoretical value of Förster resonance energy transfer efficiency (E_{theor}) was determined by the distance between energy donor and acceptor (R), the value of the spectral overlap integral (J), the value of the orientation factor (κ^2), and several other parameters. In this work the values of R and κ^2 for all possible combinations of the donor Trps and acceptor Trps were calculated from the published crystal structure of HγD-Crys (*9*). Two κ^2 values were in good agreement with those computed using a molecular dynamics simulation (*18*), while the remaining κ^2 values and R values have not been previously reported. Experimental energy transfer efficiencies were calculated from the energy transfer rates k_{12} and k_{21} using eqs 5 and 6. Table 3 shows theoretical and experimental values of the forward and reverse energy transfer efficiencies for the two Trps in the N-terminal domain and the two Trps in the C-terminal domain.

The experimental value of the forward energy transfer efficiency in the C-terminal domain was about 71%, which was higher than that in the N-terminal domain (56%). The theoretical efficiencies for the forward energy transfer were fairly close to the experimental values. The difference between the two domains in the forward energy transfer efficiency is due to the greater value of the overlap integral (J) and the higher donor quantum yield (Q_D) in the C-terminal domain than in the N-terminal domain. Theoretical energy transfer efficiencies for the reverse transfer, from quenched *Trp68* or *Trp156* to moderately fluorescent Trp42 or Trp130, do not exceed 5%. This results from the low quantum yields of *Trp68* and *Trp156*, which play the roles of the donors in the case of reverse energy transfer. Experimental values of the reverse energy transfer efficiency equal zero within experimental uncertainties.

The FRET efficiencies for two swapped Trp pairs are shown in Table 4. Both experimental and theoretical efficiency values are very close to zero when the donor and

Table 3: Calculated Overlap Integrals (J), Orientation Factors (κ^2), Donor Quantum Yields (Q_D), Förster Radii (R_0), Center-to-Center Distances (R), Forward Energy Transfer Rate (k_{12}) or Reverse Energy Transfer Rate (k_{21}), and Energy Transfer Efficiencies (E) for the Two Trps in Each Domain of HγD-Crys

	Trp pairs			
	N-terminal domain		C-terminal domain	
	Trp42→*Trp68*	*Trp68*→Trp42	Trp130→*Trp156*	*Trp156*→Trp130
J ($\times 10^{-13}$ cm^6·mol^{-1})	1.4 ± 0.3	0.87 ± 0.4	1.7 ± 0.4	1.1 ± 0.3
κ^2	0.56	0.56	0.57	0.57
Q_D[a]	0.13 ± 0.01	0.0076 ± 0.0008	0.17 ± 0.02	0.0099 ± 0.001
R_0 (Å)[b]	11.8 ± 0.5	6.8 ± 0.6	12.8 ± 0.6	7.4 ± 0.4
distance (Å)	12.2	12.2	12.4	12.4
k_{12} or k_{21} (ns^{-1})	0.51 ± 0.09	∼0[c]	0.70 ± 0.09	∼0
E_{theor} (%)[d]	44 ± 6	3 ± 1	55 ± 7	4 ± 1
E_{exper} (%)[e]	56 ± 2	∼0[c]	71 ± 2	∼0

[a] Q_D is the quantum yield determined by steady-state fluorescence using L-Trp (*18*). [b] R_0 was calculated using the Förster equation from the values of J, κ^2, Q_D, and other parameters. [c] The experimental values of the reverse energy transfer rate (k_{21}) and the reverse energy transfer efficiency (E_{exper}) equal zero within experimental uncertainties. [d] E_{theor} is the theoretical energy transfer efficiency calculated from the values of R and R_0. [e] E_{exper} is the experimental value of energy transfer efficiency calculated using eqs 5 and 6.

Table 4: Calculated Overlap Integrals (J), Orientation Factors (κ^2), Donor Quantum Yields (Q_D), Förster Radii (R_0), Center-to-Center Distances (R), and Energy Transfer Efficiencies (E) for Two Trp Pairs with the Trps in the Different Domains of HγD-Crys

	crossed Trp pairs			
	Trp42→*Trp156*	*Trp156*→Trp42	Trp130→*Trp68*	*Trp68*→Trp130
J ($\times 10^{-13}$ cm^6·mol^{-1})	1.3 ± 0.4	1.0 ± 0.4	1.8 ± 0.3	1.0 ± 0.3
κ^2	0.05	0.05	0.03	0.03
Q_D[a]	0.13 ± 0.01	0.0099 ± 0.001	0.17 ± 0.02	0.0076 ± 0.0008
R_0 (Å)[b]	7.9 ± 0.4	4.9 ± 0.3	7.8 ± 0.3	4.2 ± 0.2
distance (Å)	22.3	22.3	21.8	21.8
E_{theor} (%)[c]	0.2 ± 0.07	0.01 ± 0.005	0.2 ± 0.04	0.005 ± 0.002
E_{exper} (%)[d]	3 ± 2	−[e]	3 ± 2	−

[a] Q_D is the quantum yield determined by steady-state fluorescence using L-Trp (*18*). [b] R_0 was calculated using the Förster equation from the values of J, κ^2, Q_D, and other parameters. [c] E_{theor} is the theoretical energy transfer efficiency calculated from the values of R and R_0. [d] E_{exper} is the experimental value of energy transfer efficiency calculated using eqs 5 and 6. [e] − represents the fact that the experimental values of reverse energy transfer efficiency could not be determined.

acceptor are in the different domains (Trp42→*Trp156* and Trp130→*Trp68*). This results from large distances (R) between Trp residues in the different domains.

Time-Resolved Emission Spectra of Trp130-Only HγD-Crys. Time-resolved emission spectra (TRES) of Trp130-only HγD-Crys are shown in Figure 3. The difference between the spectra at 0 and 0.40 ns after excitation can be attributed to the short-lived contribution from tyrosine residues (see above). Likewise, the difference between the spectra at 4.00 and 10.0 ns is likely due to the solvent-exposed Trp in a trace contaminant protein. The instantaneous spectra at 0.40, 1.50, and 4.00 ns are almost identical, which shows that the time-dependent red shift is not observed with Trp130 in HγD-Crys during the time window between 0.40 and 4.00 ns. Nanosecond time-dependent red shifts are observed only if the protein has soft normal vibration modes that are coupled to the Trp static dipole moment change via the motion of charged groups or water molecules relative to the Trp side chain. At least two possible explanations of the absence of the time-dependent red shift in Trp fluorescence in a protein can be considered. First, it is possible that the protein matrix around each Trp is so rigid that the polar groups within 5 Å and charged groups within 10 Å distance from the Trp cannot move. The second possibility is that there are no charged groups and no water molecules in close proximity to the Trp side chain. In the case of HγD-Crys, the Trp130 side chain has no direct contact with water molecules. On the other hand, according to the crystal structure (*9*), the charged residues His87, Asp107, and

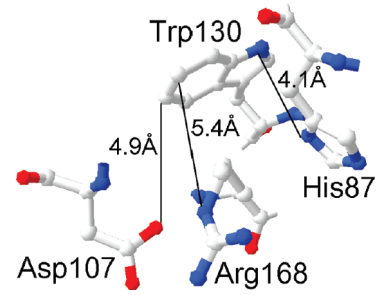

FIGURE 6: Crystal structure of charged residues close by Trp130 (PDB code: 1HK0).

Arg168 are close to Trp130 (Figure 6). The δ-nitrogen of His87 is 4.1 Å away from the indole nitrogen of Trp130. One of the carboxyl oxygen atoms of Asp107 is 4.9 Å away from the indole carbon 5 of Trp130. The δ-nitrogen of Arg168 is 5.4 Å away from the indole carbon 6 of Trp130. If the side chains of His87, Asp107, and Arg168 could move relative to the Trp130 side chain on the nanosecond time scale, then the time-dependent red shift would have been observed. Since the shift is not observed, this suggests that the protein matrix around Trps of HγD-Crys is exceptionally rigid.

Time-Resolved Fluorescence Anisotropy. For Trp42 in the N-terminal domain and Trp130 in the C-terminal domain we measured the vertical and horizontal polarization components of the time-resolved fluorescence at only one emission wavelength (340 nm). The two polarization components were fitted simultaneously by the model described

Table 5: Parameters for the Time-Resolved Anisotropy of Trp42 in the N-Terminal Domain (N-td) and Trp130 in the C-Terminal Domain (C-td)[a]

domains	proteins	β	ϕ (ns)	no. of exponentials	χ^2
N-td	Trp42-only	0.245	11.1	single	1.01
C-td	Trp130-only	0.248	11.6	single	1.05

[a] β and ϕ represent the amplitude and correlation time, respectively.

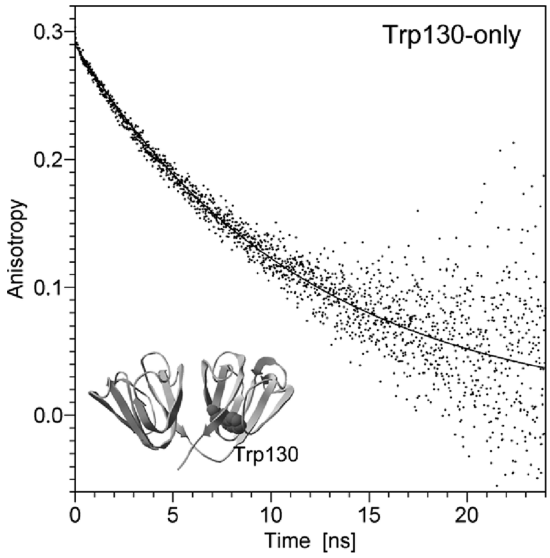

FIGURE 7: Time-resolved anisotropy of Trp130-only HγD-Crys. The solid line represents the $r(t)$ function with the best fit parameters. The ribbon structure of wild-type HγD-Crys with Trp130 in spacefill is shown at the bottom. The dots represent the anisotropy values calculated from the vertical and horizontal polarization photon counts on a channel by channel basis. Since the data shown by the dots have not been deconvoluted from the IRF, they may differ significantly from the δ excitation $r(t)$ model; however, it is difficult to see the difference because the width of the IRF (65 ps) is comparable to the width of the solid line. The dots are shown for illustrative purposes only. The data represented by the dots are not raw experimental data and were not fitted by any model. Instead, we fitted the raw vertical and horizontal polarization data as described in Materials and Methods.

in Materials and Methods. For both Trp42-only and Trp130-only adequate fits were achieved with monoexponential $r(t)$. The values of the parameters involved in $r(t)$ and the reduced global χ^2 are shown in Table 5. The time-resolved anisotropy (TRA) of Trp130-only protein is shown in Figures 7 and 8. The TRA of the Trp42-only protein is shown in Figure 11S in Supporting Information and in Figure 8. The emission of Trp130 and Trp42 dominated over the emission from tyrosines and the trace contaminant. In the cases of *Trp68-only* and *Trp156-only* proteins Trp fluorescence emission intensity was dominant only during the first 0.5 ns, and after that the signal from the trace contaminant became dominant. This means that in the TRA of *the Trp68-only* or *Trp156-only* protein only the first 0.5 ns are relevant to HγD-Crys rotational dynamics. Since the 0.5 ns time window would be too short to study the rotational dynamics of a protein with ~21 kDa molecular mass, we did not measure the TRA of *Trp68-only* and *Trp156-only* proteins.

Multiexponential $r(t)$ has been observed in many proteins (*17*). In proteins containing a single Trp residue multiexponential $r(t)$ usually is interpreted in terms of segmental motion, such as the twisting of a small flexible tail in the F3W mutant of IIA^{Glc} protein (*32*). In the case of HγD-Crys we observed monoexponential $r(t)$. Almost identical $r(t)$ was observed with Trp42-only and Trp130-only proteins (Figure 8). On the semilog plot, the monoexponential $r(t)$ shows up as straight line with slope inversely proportional to the rotational correlation time (ϕ). The values of the correlation time (ϕ) are nearly the same for Trp42-only and Trp130-only (Figure 8 and Table 5). The mass m of a spherical rotating object can be calculated from its rotational correlation time ϕ, specific gravity ρ, solvent viscosity η, Boltzmann constant k_B, and absolute temperature T, using the Stokes equation (*14*):

$$m = \frac{k_B T \rho \varphi}{\eta} \tag{14}$$

Based on the rotational correlation times from Table 5, eq 14 gives the molecular mass of 22.7 ± 0.5 kDa. Since the actual molecular mass of both Trp42-only and Trp130-only HγD-Crys is 21.7 kDa, it is most likely that in addition to the protein the rotating object also contains about 1.0 ± 0.5 kDa of water. The fact that $r(t)$ is monoexponential implies that the side chains of Trp42 or Trp130 cannot rotate about the χ_1 and χ_2 angles and there is no segmental motion. In other words, HγD-Crys is a rigid protein with tight side chain packing.

DISCUSSION

The most striking feature of Trps in HγD-Crys is their short lifetimes in the native state. In the wild-type HγD-Crys, the lifetimes of two moderately fluorescent Trps (Trp42 and Trp130) were shortened as a result of the intradomain energy transfer from Trp42 to *Trp68* in the N-terminal domain and from Trp130 to *Trp156* in the C-terminal domain. The lifetimes of *Trp68* and *Trp156* are only ~0.1 ns, which is due to the extremely fast electron transfer rates stabilized by the electrostatic environments of these two Trps. Some of the ambient UV light with wavelength above 295 nm can transmit through cornea and be absorbed by the lens (*11*). The major chromophores inside the lens absorbing near-UV light (300−400 nm) are tryptophan residues in crystallin proteins and some small molecules, such as kynurenine and 3-hydroxykynurine glucoside (*48*). The molecules that absorb near-UV radiation receive the additional energy equal to that of one photon and become electronically excited. To return to the ground state the molecules must dissipate the energy in some way, such as by breaking chemical bonds or by reradiating photons at another frequency. Covalent damage of Trp residues can lead to the indole ring cleavage, which might originate from the formation of a short-lived Trp cation radical (*49, 50*). This may cause partial unfolding of the protein and then result in protein aggregation. Nonradiative pathway (quenching) of Trps in HγD-Crys provides a deactivation channel to dissipate the energy absorbed from the ambient light. Quenching competes with the formation of Trp photoionization state and fluorescent state, and thus it can minimize the chance of photochemical reaction of Trps.

Time-Resolved Fluorescence Measurements. The time-resolved data obtained with the triple Trp to Phe substitutions of HγD-Crys (Trp42-only, *Trp68-only*, Trp130-only, and *Trp156-only*) made it possible to determine the mean lifetimes of individual Trps and to answer important questions regarding heterogeneity and relaxation. The data from

two different double Trp to Phe substitutions of HγD-Crys (Trp42/*Trp68* and Trp130/*Trp156*) made it possible to evaluate the effect of the presence of the energy acceptors on the mean lifetimes of the energy donors, which provided accurate values of the energy transfer efficiencies for each donor−acceptor pair. Steady-state measurements alone could not provide accurate values of the energy transfer efficiencies because when both the donors and the acceptors are Trp, they emit in the same spectral range. The time-resolved measurements made it possible to separate the signals from the donor and the acceptor based on a very large difference between the mean lifetimes of the donors (~3 ns) and the acceptors (~0.1 ns).

Heterogeneity and Relaxation. Electrostatic solvation of solvatochromic fluorophores (such as Trp) in a polar solvent or in a protein matrix results in a continuous time-dependent red shift of the instantaneous emission spectrum, but it does not cause a significant deviation of the excited-state population decay from the monoexponential law. This must produce negative values of $\alpha_n(\lambda)$ on the red side of the emission peak for at least some of the exponential terms. The negative amplitudes have been observed in several single-Trp proteins (*32, 33*). However, the negative amplitudes have not been observed with any of the four Trp residues in HγD-Crys, which clearly shows that electrostatic solvation of Trp residues in the protein matrix is not an important player in the case of HγD-Crys. The lack of the characteristic time-dependent red shift in the emission of single-Trp-containing proteins also indicates that no significant electrostatic solvation takes place in this protein. We attribute this to the exceptional rigidity of the HγD-Crys.

Strong deviations of the population decay from the monoexponential law are expected in those cases where a configuration-dependent dynamic quenching mechanism is present. Since electron transfer from an excited-state Trp residue to a protein backbone depends on the overlap of electronic orbitals between the Trp residue and the backbone, the quenching rate associated with the transfer is a function of the distance between the Trp residue and the backbone. The rate of electron transfer also depends on the local electric field, which may stabilize or destabilize the charge transfer (CT) state (*24*). Random vibrations of amino acid side chains modulate the distance between the Trp residue and the backbone, as well as the local electric field. These vibrations happen on the same time scale (10−100 ps) as the decay of the highly quenched Trp residues in HγD-Crys, which results in a significantly nonexponential decay law. The exact shape of the decay law can be obtained by solving the partial differential equations that describe molecular diffusion and population decay. Any nonexponential decay law can be approximated by a linear combination of a few exponential terms. The total number of terms required for an adequate approximation is usually between two and six, depending on the desired accuracy of approximation.

If the deviation of the time-resolved fluorescence emission from the monoexponential law is caused by a combination of the Brownian motion with a configuration-dependent dynamic quenching mechanism, then the time constants τ_n are not associated with the decays of different excited-state populations, and they should not be called the decay times or lifetimes. Likewise, the spectra $\alpha_n(\lambda)$ or $\alpha_n(\lambda)\cdot\tau_n$ do not represent the decay-associated spectra. Since the configuration-dependent quenching is not directly correlated with a spectral shift, no negative amplitudes are anticipated, and all preexponential amplitude spectra $\alpha_n(\lambda)$ are expected to have their peaks at about the same wavelength. This situation is observed in the cases of *Trp68-only* and *Trp156-only*. For example, in the case of *Trp156-only*, the amplitude spectra associated with the 50, 116, and 272 ps exponentials have similar shapes (see Figure 4S in the Supporting Information). The spectra associated with the 1.43, 4.00, and 7.58 ns have their peaks at different wavelengths; on the basis of this observation and on the tiny amplitudes of these spectra we attributed them to Tyr emission and to impurities present in the sample in trace amounts. The fluorescence from these trace impurities is usually negligible as compared to the fluorescence of high quantum yield Trp residues, but it becomes detectable when we look at the fluorescence of the highly quenched Trp residues like *Trp68* and *Trp156*.

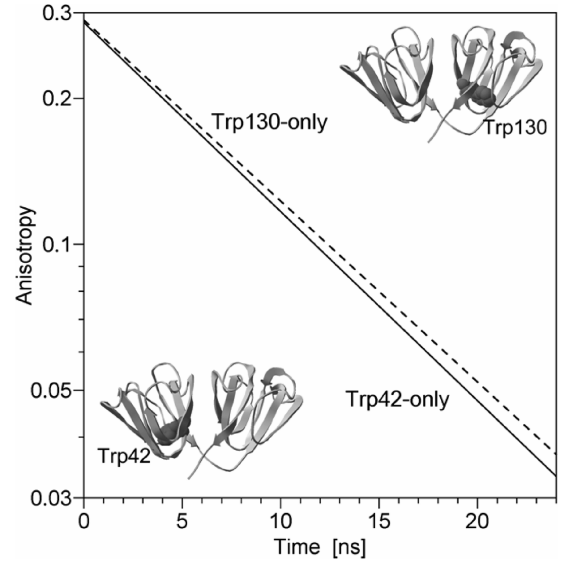

FIGURE 8: Semilog plots of the best fit of time-resolved anisotropy models for Trp42-only and Trp130-only HγD-Crys. The ribbon structure of wild-type HγD-Crys with Trp130 in spacefill is shown at the upper right corner and the one with Trp42 in spacefill is shown at the bottom. The solid line represents the time-resolved anisotropy of Trp42 in the N-terminal domain, and the broken line represents the time-resolved anisotropy of Trp130 in the C-terminal domain.

Time Constants τ_n of Multiple-Trp-Containing Proteins. Multiexponential time-resolved fluorescence emission has been often observed even for the single-Trp-containing proteins (*17*). If the proteins contain more than one Trp, then each time constant cannot be simply assigned to individual Trp without enough experimental evidence. The study of a series of Trp mutants of HγD-Crys demonstrated that the multiple exponential terms in proteins containing multiple Trps can be accurately assigned to each Trp in some cases, if the time-resolved emission of single-Trp proteins has been studied and the time constants corresponding to different Trps differ by an order of magnitude or more. For example, in the double-Trp mutant, *Trp68*/Trp130, the two exponential terms with time constants of 65 and 169 ps could be attributed to *Trp68*, and the two exponential terms with time constants of 1.45 and 3.15 ns could be attributed to Trp130.

In the presence of intradomain energy transfer between two Trps (Trp42/*Trp68* and Trp130/*Trp156*), which have been discussed in previous section, the mean lifetime of the

donor (Trp42 or Trp130) was shortened, but all of the time constants τ_n attributable to the donor were still considerably longer than those attributable to the acceptor. Thus, it was possible to separate the donor exponentials from the acceptor exponentials. If no interaction occurred between two Trps, then there would be two possible situations. First, if the shortest τ_n for one Trp (e.g., Trp42 or Trp130) was at least three times longer than the longest τ_n for the other Trp (e.g., *Trp156* or *Trp68*), then the instrument would be able to resolve the signals from these two Trps (e.g., Trp42/*Trp156* or *Trp68*/Trp130). Second, if the time constants of two Trps were very close, e.g., Trp42/Trp130 or *Trp68*/*Trp156*, then the instrument would not be able to resolve the exponential terms associated with the individual Trps. In the latter case the number of the resolved exponential terms for the double mutants was the same as the number of the exponential terms for either single-Trp-containing protein. For example, six exponential terms were necessary to fit the time-resolved emission from *Trp68-only* and *Trp156-only*, and also six exponential terms were sufficient to fit the time-resolved emission of *Trp68*/*Trp156*. In this case the time constants τ_n could not be called lifetimes or attributed to either Trp residue, whereas the sum of all exponential terms gave an excellent global fit to the time-resolved emission of the double-Trp protein in every part of the emission spectrum.

Multiexponential Fluorescence of Trps and Charge Transfer Mechanism. The short mean lifetimes for *Trp68* and *Trp156* are consistent with their very low quantum yields computed by QM-MM methods developed by Callis et al. (*18, 24*−*29*). Compared to moderately fluorescent Trp42 and Trp130, the extreme quenching of *Trp68* and *Trp156* arises essentially from their smaller CT−^1L_a energy gap and the larger fluctuations (*18*). When the energy gap is small and fluctuations are large, the probability that the fluorescing and CT states will have the same energy is high. The quenching will occur under this circumstance because electron transfer (the quenching process) is only possible when the fluorescing and CT states have the same energy (*24*). The energy of the CT state depends on the local electric field, and so is the electron transfer rate. In addition, the transfer rate depends on the distance between the Trp side chain and the protein backbone. Random Brownian motions of protein and solvent atoms are responsible for both the CT state energy fluctuations and Trp backbone distance fluctuations. Molecular dynamics (MD) simulations reveal that there are fluctuations lasting ~0.02 ns that conceivably could attribute to the two exponential terms (0.061 and 0.144 ns) of *Trp68* and three exponential terms (0.050, 0.116, and 0.272 ns) of *Trp156*.

The highest fluorescence quantum yields for single Trps in proteins are normally close to 0.3 (*24*), a value that varies only slightly depending on the polarity of the environment. The quantum yield (0.13) of Trp42 suggested there is moderate electron transfer quenching, but the electron transfer rate is much less than *Trp68* or *Trp156* due to the difference in their electrostatic environments. The more fluorescent Trp42 has two exponential terms, 2.85 and 1.72 ns, with amplitudes of 68% and 25%, respectively. The 1.72 ns exponential could possibly be attributable to the fluctuation of the CT−^1L_a energy gap of Trp42.

Time-Resolved Fluorescence Anisotropy. Time-resolved anisotropy of the fluorescence emission from a probe attached to a protein molecule can provide information about the size of the macromolecule, about its flexibility, and whether the side chain packaging in the environment of the fluorescent probe is tight or loose. During the analysis of the time-resolved anisotropy data we approximate the time-resolved anisotropy by a linear combination of exponential terms as described in eq 2. The resulting exponential terms $\beta_n \exp(-t/\phi_n)$ are then sorted in accordance with the values of the rotational correlation times ϕ_n. The rotation of the protein as a whole should result in the rotational correlation time (*14*):

$$\varphi_0 = \frac{\eta V_1}{k_B T} \tag{15}$$

where η is the solvent viscosity, V_1 is the volume of one protein molecule, including the volume of water trapped in internal cavities or tightly bound to protein surface, k_B is the Boltzmann constant, and T is the absolute temperature. If the protein molecule is not spherical (i.e., rod-like or disk-like), then instead of one rotational correlation time ϕ_0 we expect up to three rotational correlation times ϕ_1, ϕ_2, ϕ_3. The longest and the shortest of these three ϕ_n differ by less than 50%; therefore, in practice the three exponential terms resulting from the nonspherical shape of a protein molecule cannot be resolved from the experimental data. In contrast to that, segmental motions of protein domains or secondary structure elements result in rotational correlation times ϕ_n that are much shorter than ϕ_0 given by eq 15. For example, if the mass of the whole protein is N times greater than the mass of the rotating segment, then the rotational correlation time for the segment can be roughly estimated as ϕ_0/N. For $N > 3$ it should be easy to separate the exponential term corresponding to segmental motion from the one describing the rotation of the protein as a whole. Furthermore, if the side chain packing in the environment of the fluorescent probe is not tight, then the rotation of the fluorescent probe about a flexible linker arm should be observed. In our experiments the moderately fluorescent Trp residues in Trp42-only and Trp130-only were used as the fluorescent probes. The rotation of the Trp side chain about the $C_\alpha-C_\beta$ bond and $C_\beta-C_\gamma$ bond can result in exponential terms with ϕ_n ~100 ps (*51*). In the case of Trp42-only and Trp130-only HγD-Crys we did not observe exponential terms with ϕ_n ~100 ps, which is indicative of very tight side chain packing in the vicinity of the Trp residues. The observed time-resolved anisotropy was monoexponential; therefore, no segmental motion of any kind was detected in HγD-Crys. This shows that HγD-Crys is a rigid molecule, containing no loose segments or secondary structure elements that could move significantly relative to the rest of the molecule.

Ocular Lens Protects Retina from Near-UV Radiation. In the human eye, the retina is very sensitive to UV radiation and is damaged by exposure to it. The cornea efficiently blocks the UV light with wavelength below 295 nm, but the lens is the major filter for near-UV light (300−400 nm). Trps in crystallin proteins and some other tryptophan derivatives inside the lens (e.g., kynurenine and 3-hydroxykynurenine) can both absorb UV and therefore prevent UV light from reaching the retina. Even though the Trp absorbance from 300 to 320 nm is only the tail of its UV absorption spectrum (*14*), considering the high protein concentration inside the lens, these portions are very important to shield the retina

from UV light. Near-UV light can damage the retina photoreceptor in a lensless eye in the animal models (*52, 53*). Surgical removal of a cataract results in the loss of the natural lens filter. Without appropriate implant of intraocular lens during cataract surgery, the retina can be damaged by ultraviolet energy from solar radiation (*54*). For some patients with cataract surgery, the retina became more vulnerable to near-UV exposure (*55*), and there is an increased risk of age-related macular degeneration (*56, 57*), which has been implicated as a consequence of photooxidative retina light damage (*58*).

Properties of Trp in γ-Crystallin May Be Important To Protect Themselves from UV-Induced Photoreactions. If absorption of UV radiation by lens crystallins protects the retina, the crystallins themselves would be subject to UV photodamage. Excessive UV-B exposure is one of the risk factors for cataract formation (*59*). The World Health Organization estimated that UV radiation is directly responsible for 5% of cataract-related disease (*60*). Even though the cornea can absorb almost all the light of wavelength shorter than 295 nm, there is about 24 mW/cm^2 sunlight in the range of 300−400 nm which reaches the human lens (*61*). Cataract formation was observed in certain animal models exposed to the near-UV light (300−400 nm). One of the causative factors could be chemical alterations in the Trp residues of crystallin proteins or free Trp in the lens (*61*). The young crystallin lenses transmit about 75% UV (300−400 nm), while the corresponding UV transmission dropped dramatically to 20% in the yellowish aged lenses due to the accumulations of small UV filters, such as 3-hydroxykynurenine glucoside (*62, 63*). The unique properties of Trps in HγD-Crys, including their highly hydrophobic environments, efficient quenching of the fluorescence intensity (short lifetimes), and no segmental motion around Trps, might have been evolved in crystallin fold to protect Trp residues from photoinduced reactions.

The Trps in HγD-Crys are highly buried inside the hydrophobic core of the β-sheet fold. Solvent-exposed Trps are more susceptible to photooxidation than buried Trp in proteins (*64*). Trp residues in a hydrophobic environment were photolyzed at a slower rate than those that were solvent exposed (*65*). Similar trends have also been observed for bovine crystallins. Bovine αB-crystallin contains two Trps, Trp9 and Trp60. The photolysis rate of Trp9 is more rapid than Trp60 under UV radiation at 308 nm (*31*). This was explained by more solvent exposure area of Trp9 than Trp60.

The short lifetimes of Trp in HγD-Crys might also minimize the chance of photochemical reaction of Trps. Tallmadge et al. irradiated bovine γB-crystallin at 295 nm with 0.7 mW/cm^2 output (*66*). The photoreaction rates of moderately fluorescent Trp42 and Trp130 are much faster than quenched *Trp68* and *Trp156*. The photodamage rate of Trp42 is particularly fast among the four Trps. Based on the results of time-resolved fluorescence measurements of HγD-Crys, the lifetime of Trp42 is more than 10 times longer than *Trp68* and *Trp156*. It is likely that Trp42 has a higher chance to get into the photooxidation pathway than the quenched *Trp68* and *Trp156*.

CONCLUSION

The excited-state lifetimes of the four Trp residues in HγD-Crys were measured individually in the absence and in the presence of other Trp residues. The mean fluorescence lifetimes of *Trp68-only* and *Trp156-only* are always very short (∼0.1 ns), indicating that these residues are highly quenched. We have previously shown that electron transfer to the protein backbone is the dominant quenching mechanism for *Trp68* and *Trp156* (*18*). In contrast, the lifetimes of Trp42-only and Trp130-only are ∼3 ns, which shows that Trp42 and Trp130 are moderately fluorescent in the absence of the resonance energy transfer. The lifetime of Trp42 (or Trp130) decreases to ∼1 ns in the presence of *Trp68* (or *Trp156*). This confirms the presence of the intradomain resonance energy transfer, from Trp42 to *Trp68* in the N-terminal domain and from Trp130 to *Trp156* in the C-terminal domain. The experimental value of energy transfer efficiency is 56% in the N-terminal domain and 71% in the C-terminal domain, which is very close to those values calculated theoretically using the Förster equation and the crystal structure of the protein. No experimental evidence of interdomain energy transfer was found. Time-resolved fluorescence anisotropy data indicate that the whole protein molecule moves as one rigid body; therefore, protein domains and secondary structure elements cannot substantially move relative to one another. Also, the anisotropy data reveal no rotation of Trp side chains about the $C_\alpha-C_\beta$ and $C_\beta-C_\gamma$ bonds, which leads us to the conclusion that the environment around Trps is exceptionally rigid. We speculate that the shortening of Trp lifetimes in the wild-type HγD-Crys and the rigidity of protein might have evolved as properties of the γ-crystallin fold to protect Trps from photodegradation reactions induced by ambient UV light.

ACKNOWLEDGMENT

We thank Prof. Patrik R. Callis in Montana State University for helpful discussions and suggestions.

SUPPORTING INFORMATION AVAILABLE

Figures 1S−10S showing preexponential amplitude spectra $\alpha_i(\lambda)$ of different Trp mutants (Trp42-only, *Trp68-only*, Trp42/*Trp68*, *Trp156-only*, Trp130/*Trp156*, Trp42/*Trp156*, *Trp68*/Trp130, Trp42/Trp130, and *Trp68*/*Trp156*) and wild-type HγD-Crys; Figure 11S showing the time-resolved anisotropy of Trp42-only HγD-Crys; Table 1S showing the coordinates of the centers and the directions of transition dipole moments for all Trps; Table 2S showing the calculated values of R and κ^2 for Trp pairs of HγD-Crys; equations (1−6) showing the calculation of the mean lifetime for each Trp. This material is available free of charge via the Internet at http://pubs.acs.org.

REFERENCES

1. Augusteyn, R. C. (2004) alpha-crystallin: a review of its structure and function. *Clin. Exp. Optom. 87*, 356–366.
2. Reddy, G. B., Kumar, P. A., and Kumar, M. S. (2006) Chaperone-like activity and hydrophobicity of alpha-crystallin. *IUBMB Life 58*, 632–641.
3. Oyster, C. (1999) *The human eye: structure and function. Chapter 12: The lens and the vitreous*, Sinauer Associates, Inc., Sunderland, MA.
4. Hanson, S. R., Hasan, A., Smith, D. L., and Smith, J. B. (2000) The major in vivo modifications of the human water-insoluble lens crystallins are disulfide bonds, deamidation, methionine oxidation and backbone cleavage. *Exp. Eye Res. 71*, 195–207.

5. Hanson, S. R., Smith, D. L., and Smith, J. B. (1998) Deamidation and disulfide bonding in human lens gamma-crystallins. *Exp. Eye Res. 67*, 301–312.
6. Hains, P. G., and Truscott, R. J. (2007) Post-translational modifications in the nuclear region of young, aged, and cataract human lenses. *J. Proteome Res. 6*, 3935–3943.
7. Searle, B. C., Dasari, S., Wilmarth, P. A., Turner, M., Reddy, A. P., David, L. L., and Nagalla, S. R. (2005) Identification of protein modifications using MS/MS de novo sequencing and the OpenSea alignment algorithm. *J. Proteome Res. 4*, 546–554.
8. Lampi, K. J., Ma, Z., Shih, M., Shearer, T. R., Smith, J. B., Smith, D. L., and David, L. L. (1997) Sequence analysis of betaA3, betaB3, and betaA4 crystallins completes the identification of the major proteins in young human lens. *J. Biol. Chem. 272*, 2268–2275.
9. Basak, A., Bateman, O., Slingsby, C., Pande, A., Asherie, N., Ogun, O., Benedek, G. B., and Pande, J. (2003) High-resolution X-ray crystal structures of human gammaD crystallin (1.25 Å) and the R58H mutant (1.15 Å) associated with aculeiform cataract. *J. Mol. Biol. 328*, 1137–1147.
10. McCarty, C. A., and Taylor, H. R. (2002) A review of the epidemiologic evidence linking ultraviolet radiation and cataracts. *Dev. Ophthalmol. 35*, 21–31.
11. Lerman, S. (1980) *Radiant energy and the eye. Chapter 3: Biological and chemical effects of ultraviloet radiation*, Macmillan Publishing, New York.
12. Merriam, J. C., Lofgren, S., Michael, R., Soderberg, P., Dillon, J., Zheng, L., and Ayala, M. (2000) An action spectrum for UV-B radiation and the rat lens. *Invest. Ophthalmol. Visual Sci. 41*, 2642–2647.
13. Soderberg, P. G., Lofgren, S., Ayala, M., Dong, X., Kakar, M., and Mody, V. (2002) Toxicity of ultraviolet radiation exposure to the lens expressed by maximum tolerable dose, in *Progress in lens and cataract research* (Hockwin, O., Kojima, M., Takahashi, N., and Sliney, D. H., Eds.) pp 70−75, S. Karger, Basel.
14. Lakowicz, J. (1999) *Principles of fluorescence spectroscopy*, 2nd ed., Kluwer Academic/Plenum, New York.
15. Kurzel, R. B., Wolbarsht, M., Yamanashi, B. S., Staton, G. W., and Borkman, R. F. (1973) Tryptophan excited states and cataracts in the human lens. *Nature 241*, 132–133.
16. Creed, D. (1984) The photophysics and photochemistry of the near-UV absorbing amino acids-I. Tryptophan and its simple derivatives. *Photochem. Photobiol. 39*, 537–562.
17. Beechem, J. M., and Brand, L. (1985) Time-resolved fluorescence of proteins. *Annu. Rev. Biochem. 54*, 43–71.
18. Chen, J., Flaugh, S. L., Callis, P. R., and King, J. (2006) Mechanism of the highly efficient quenching of tryptophan fluorescence in human gammaD-crystallin. *Biochemistry 45*, 11552–11563.
19. Bateman, O. A., Sarra, R., van Genesen, S. T., Kappe, G., Lubsen, N. H., and Slingsby, C. (2003) The stability of human acidic beta-crystallin oligomers and hetero-oligomers. *Exp. Eye Res. 77*, 409–422.
20. Liang, J. J. (2004) Interactions and chaperone function of alphaA-crystallin with T5P gammaC-crystallin mutant. *Protein Sci. 13*, 2476–2482.
21. Kim, Y. H., Kapfer, D. M., Boekhorst, J., Lubsen, N. H., Bachinger, H. P., Shearer, T. R., David, L. L., Feix, J. B., and Lampi, K. J. (2002) Deamidation, but not truncation, decreases the urea stability of a lens structural protein, betaB1-crystallin. *Biochemistry 41*, 14076–14084.
22. Wenk, M., Herbst, R., Hoeger, D., Kretschmar, M., Lubsen, N. H., and Jaenicke, R. (2000) Gamma S-crystallin of bovine and human eye lens: solution structure, stability and folding of the intact two-domain protein and its separate domains. *Biophys. Chem. 86*, 95–108.
23. Das, B. K., and Liang, J. J. (1998) Thermodynamic and kinetic characterization of calf lens gammaF-crystallin. *Int. J. Biol. Macromol. 23*, 191–197.
24. Callis, P., and Liu, T. (2004) Quantitative predictions of fluorescence quantum yields for tryptophan in proteins. *J. Phys. Chem. B 108*, 4248–4259.
25. Callis, P., and Vivian, J. (2003) Understanding the variable fluorescence quantum yield of tryptophan in proteins using QM-MM simulations. Quenching by charge transfer to the peptide backbone. *Chem. Phys. Lett. 369*, 409–414.
26. Kurz, L. C., Fite, B., Jean, J., Park, J., Erpelding, T., and Callis, P. (2005) Photophysics of tryptophan fluorescence: link with the catalytic strategy of the citrate synthase from Thermoplasma acidophilum. *Biochemistry 44*, 1394–1413.
27. Liu, T., Callis, P. R., Hesp, B. H., de Groot, M., Buma, W. J., and Broos, J. (2005) Ionization potentials of fluoroindoles and the origin of nonexponential tryptophan fluorescence decay in proteins. *J. Am. Chem. Soc. 127*, 4104–4113.
28. Xu, J., Toptygin, D., Graver, K. J., Albertini, R. A., Savtchenko, R. S., Meadow, N. D., Roseman, S., Callis, P. R., Brand, L., and Knutson, J. R. (2006) Ultrafast Fluorescence Dynamics of Tryptophan in the Proteins Monellin and IIA(Glc). *J. Am. Chem. Soc. 128*, 1214–1221.
29. Callis, P. R., Petrenko, A., Muino, P. L., and Tusell, J. R. (2007) Ab initio prediction of tryptophan fluorescence quenching by protein electric field enabled electron transfer. *J. Phys. Chem. B 111*, 10335–10339.
30. Borkman, R. F., Douhal, A., and Yoshihara, K. (1993) Picosecond fluorescence decay of lens protein gamma-II crystallin. *Biophys. Chem. 47*, 203–211.
31. Borkman, R. F., Douhal, A., and Yoshihara, K. (1993) Picosecond fluorescence decay in photolyzed lens protein alpha-crystallin. *Biochemistry 32*, 4787–4792.
32. Toptygin, D., Savtchenko, R. S., Meadow, N. D., and Brand, L. (2001) Homogeneous spectrally- and time-resolved fluorescence emission from single-tryptophan mutants of IIA(Glc) protein. *J. Phys. Chem. B 105*, 2043–2055.
33. Toptygin, D., Gronenborn, A. M., and Brand, L. (2006) Nanosecond relaxation dynamics of protein GB1 identified by the time-dependent red shift in the fluorescence of tryptophan and 5-fluorotryptophan. *J. Phys. Chem. B 110*, 26292–26302.
34. Ross, J. B. A., Rousslang, K. W., and Brand, L. (1981) Time-Resolved Fluorescence and Anisotropy Decay of the Tryptophan in Adrenocorticotropin-(1−24). *Biochemistry 20*, 4361–4369.
35. Kosinski-Collins, M. S., Flaugh, S. L., and King, J. (2004) Probing folding and fluorescence quenching in human gammaD crystallin Greek key domains using triple tryptophan mutant proteins. *Protein Sci. 13*, 2223–2235.
36. Gill, S. C., and von Hippel, P. H. (1989) Calculation of protein extinction coefficients from amino acid sequence data. *Anal. Biochem. 182*, 319–326.
37. Hamilton, W. C. (1964) *Statistics in physical science. Estimation, hypothesis testing, and least squares*, Ronald Press, New York.
38. Knutson, J. R., Beechem, J. M., and Brand, L. (1983) Simultaneous Analysis of Multiple Fluorescence Decay Curves—a Global Approach. *Chem. Phys. Lett. 102*, 501–507.
39. Porter, G. B. (1972) Reversible energy transfer. *Theor. Chim. Acta (Berlin) 24*, 265–270.
40. Willaert, K., Loewenthal, R., Sancho, J., Froeyen, M., Fersht, A., and Engelborghs, Y. (1992) Determination of the excited-state lifetimes of the tryptophan residues in barnase, via multifrequency phase fluorometry of tryptophan mutants. *Biochemistry 31*, 711–716.
41. Forster, T. (1959) Transfer mechanisms of electronic excitation. *Discuss. Faraday Soc. 27*, 7–17.
42. Washburn, E. W. (1926−1930) *International Critical Tables of Numerical Data, Physics, Chemistry and Technology*, New York and London.
43. Callis, P. R. (1991) Molecular-Orbital Theory of the ^1L_b and ^1L_a States of Indole. *J. Chem. Phys. 95*, 4230–4240.
44. Callis, P. R. (1997) ^1L_a and ^1L_b transitions of tryptophan: applications of theory and experimental observations to fluorescence of proteins. *Methods Enzymol. 278*, 113–150.
45. Valeur, B., and Weber, G. (1977) Resolution of the fluorescence excitation spectrum of indole into the ^1L_a and ^1L_b excitation bands. *Photochem. Photobiol. 25*, 441–444.
46. Toptygin, D., and Brand, L. (2000) Spectrally- and time-resolved fluorescence emission of indole during solvent relaxation: a quantitative model. *Chem. Phys. Lett. 322*, 496–502.
47. Gafni, A., and Brand, L. (1976) Fluorescence Decay Studies of Reduced Nicotinamide Adenine-Dinucleotide in Solution and Bound to Liver Alcohol-Dehydrogenase. *Biochemistry 15*, 3165–3171.
48. Streete, I. M., Jamie, J. F., and Truscott, R. J. (2004) Lenticular levels of amino acids and free UV filters differ significantly between normals and cataract patients. *Invest. Ophthalmol. Visual Sci. 45*, 4091–4098.
49. Bent, D. V., and Hayon, E. (1975) Excited state chemistry of aromatic amino acids and related peptides. III. Tryptophan. *J. Am. Chem. Soc. 97*, 2612–2619.
50. Bryant, F. D., Santus, R., and Grossweiner, L. I. (1975) Laser Flash-Photolysis of Aqueous Tryptophan. *J. Phys. Chem. 79*, 2711–2716.

51. Toptygin, D., Wen, X., Barrick, D., and Brand, L. (2007) Time-resolved fluorescence of individual Trp residues in ordered and disordered regions of the Drosophila Notch receptor, paper presented at the Biophysical Society meeting, Long Beach, CA.
52. Li, Z. L., Tso, M. O., Jampol, L. M., Miller, S. A., and Waxler, M. (1990) Retinal injury induced by near-ultraviolet radiation in aphakic and pseudophakic monkey eyes. A preliminary report. *Retina 10*, 301–314.
53. Ham, W. T., Jr., Mueller, H. A., Ruffolo, J. J., Jr., Guerry, D., III, and Guerry, R. K. (1982) Action spectrum for retinal injury from near-ultraviolet radiation in the aphakic monkey. *Am. J. Ophthalmol. 93*, 299–306.
54. Werner, J. S., and Spillmann, L. (1989) UV-absorbing intraocular lenses: safety, efficacy, and consequences for the cataract patient. *Graefes Arch. Clin. Exp. Ophthalmol. 227*, 248–256.
55. Berler, D. K., and Peyser, R. (1983) Light intensity and visual acuity following cataract surgery. *Ophthalmology 90*, 933–936.
56. Pollack, A., Marcovich, A., Bukelman, A., and Oliver, M. (1996) Age-related macular degeneration after extracapsular cataract extraction with intraocular lens implantation. *Ophthalmology 103*, 1546–1554.
57. Liu, I. Y., White, L., and LaCroix, A. Z. (1989) The association of age-related macular degeneration and lens opacities in the aged. *Am. J. Public Health 79*, 765–769.
58. Zigman, S. (1993) Ocular light damage. *Photochem Photobiol. 57*, 1060–1068.
59. Robman, L., and Taylor, H. (2005) External factors in the development of cataract. *Eye 19*, 1074–1082.
60. (2006) Global disease burden from solar ultraviolet radiation, in *WHO*, WHO sites, Media centre, Fact sheets.
61. Zigman, S. (1977) Near UV light and cataracts. *Photochem. Photobiol. 26*, 437–441.
62. Lerman, S., Kuck, J. F., Jr., Borkman, R., and Saker, E. (1976) Accleration of an aging parameter (fluorogen) in the ocular lens. *Ann. Ophthalmol. 8*, 558–561.
63. Heyningen, R. V. (1973) The glucoside of 3OH-kynurenine and other fluorescent compounds in human lens, paper presented at the Ciba Foundation Symposium, Amsterdam.
64. Pigault, C., and Gerard, D. (1984) Influence of the location of tryptophanyl residues in proteins on their photosensitivity. *Photochem. Photobiol. 40*, 291–297.
65. Jori, G., and Galiazzo, G. (1971) Proflavine-sensitized selective photooxidation of the tryptophyl residues in papain. *Photochem. Photobiol. 14*, 607–619.
66. Tallmadge, D. H., and Borkman, R. F. (1990) The rates of photolysis of the four individual tryptophan residues in UV exposed calf gamma-II crystallin. *Photochem. Photobiol. 51*, 363–368.

BI800499K